SECTION III. TASK 3. COMPREHENSIVE MODEL DEVELOPMENT AND EVALUATION

Objectives

The objective of this task is to integrate advanced chemistry and physics submodels into a comprehensive two-dimensional model of entrained-flow reactors (PCGC-2) and to evaluate the model by comparing with data from well-documented experiments. Approaches for the comprehensive modeling of fixed-bed reactors will also be reviewed and evaluated and an initial framework for a comprehensive fixed-bed code will be employed after submission of a detailed test plan (Subtask 3.b).

Task Outline

This task is being performed in three subtasks. The first covers the full 72 months of the program and is devoted to the development of the entrained-bed code. The second subtask is for fixed-bed reactors and is divided into two parts. The first part (12 months) was devoted to reviewing the state-of-the-art in fixed-bed reactors. This led to the development of the research plan for fixed-bed reactors, which was approved. The code development is being done in the remaining 60 months of the program. The third subtask is to generalize the entrained-bed code to fuels other than dry pulverized coal and will be performed during the last 36 months of the program.

III.A. SUBTASK 3.A. - INTEGRATION OF ADVANCED SUBMODELS INTO ENTRAINED-FLOW CODE, WITH EVALUATION AND DOCUMENTATION

Senior Investigators - B. Scott Brewster and L. Douglas Smoot

Brigham Young University
Provo, UT 84602
(801) 378-6240 and 4326

Research Assistants - Ziaul Huque and Susana K. Berrondo

Objectives

The objectives of this subtask are 1) to integrate the FG-DVC submodel into PCGC-2, 2) incorporate additional submodels and improvements developed under Task 2, 3) evaluate the improved code, 4) improve user-friendliness and robustness, and 5) document the code.

Accomplishments

Work continued during the past year on integrating the FG-DVC submodel, evaluating the code, and improving user-friendliness and robustness. In addition, the minimum specifications for a foundational, entrained-bed code that will satisfy the terms of the contract were identified.

FG-DVC Integration

A new version of the FG-DVC submodel, with rank-dependent kinetics, was incorporated into PCGC-2. It was noticed with the new version that the sum of the functional group amounts calculated by FG-DVC does not exactly equal the total coal mass calculated by PCGC-2. Results of a typical calculation are shown in Fig. III.A-1. The difference is attributed to numerics. FG-DVC uses a simple Euler method while PCGC-2 uses a predictor-corrector method. Attempts to bring the two predictions into agreement by reducing the time step were not completely successful, although the discrepancy was reduced. In order to make the two models consistent, the coal mass in PCGC-2 is set equal to the sum of the functional group amounts calculated by FG-DVC.

Code Evaluation

Data from six reactors have been identified for code evaluation: 1) the AFR transparent wall reactor (TWR), 2) the BYU/ACERC controlled-profile reactor (CPR), 3) the 2-D furnace at Imperial College, 4) the BYU gasifier, 5) the drop-

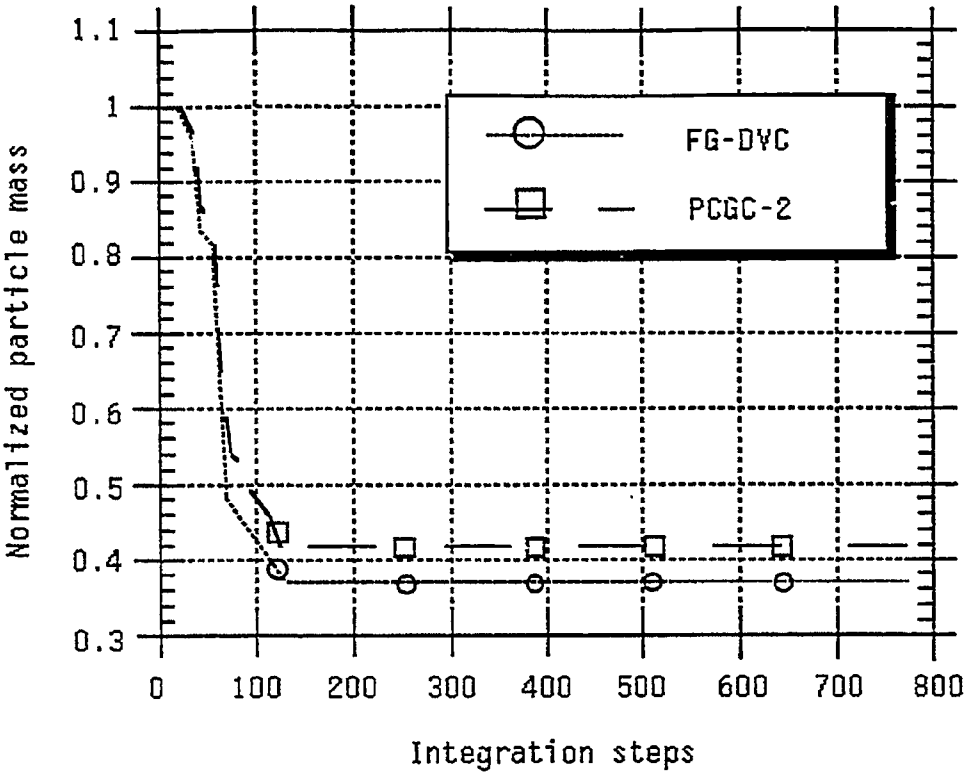

Figure III.A-1. Comparison of normalized particle mass predicted by FG-DVC and PCGC-2 for a 60-μm Rosebud coal particle in the AFR transparent wall reactor.

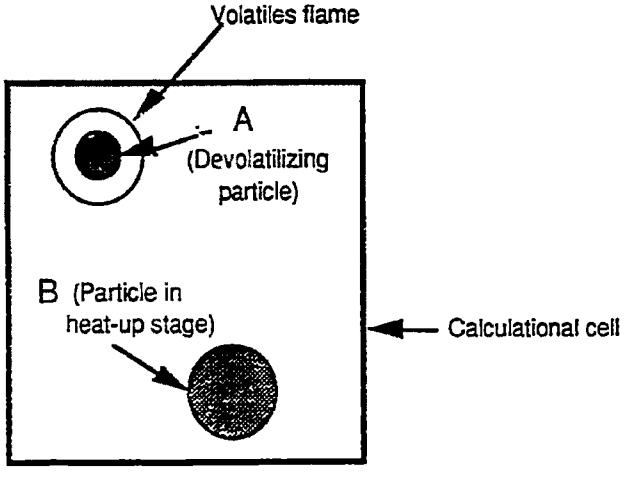

Figure III.A-2. Calculational cell in PCGC-2 showing a devolatilizing particle surrounded by burning volatiles and a non-devolatilizing particle in the same cell that is still in the heat-up stage.

tube reactor of ABB Combustion Engineering, and 6) the 80 MWe Goudey Station at Johnson City, New York, operated by New York State Electricity and Gas (NYSEG). Only near-burner test data, where the flow might be two-dimensional, will be used from the Goudey furnace. These reactors have all been simulated with PCGC-2 as described below. Simulations during the past year were performed with a simple, empirical weight-loss model for devolatilization, with kinetics reported by Solomon et al. (1986), to establish a base. Cases will be compared to subsequent predictions with PCGC-2/FG-DVC.

Transparent Wall Reactor (TWR) - Data have been received from AFR for gaseous (non-reacting) flow and three coal flames (Rosebud "fast" flow, Rosebud "slow" flow, and Pittsburgh No. 8) (Markham and Serio, 1990). Simulations of the gaseous flow case and Rosebud "fast" flow flame were described in the 4th Annual Report (Brewster et al., 1990), where the following discrepancies between measured and predicted particle temperatures were noted:

1. Predicted particles heat more rapidly than the measured particles near the edge of the stream.

2. Measured particles seem to jump more quickly in temperature when they ignite. (There is nearly 1000 degrees K difference in temperature between ignited and unignited particles at the same location.)

3. At the observed ignition point (10 cm), the predicted core is still fairly cool (1000 K) and the particles are unignited, while tomography data indicate 20 percent of the particles ignited on the centerline.

Modeling deficiencies which might account for these discrepancies include neglecting direct energy feedback from (1) volatiles combustion in the vicinity of devolatilizing coal particles, and (2) CO_2 formation in the vicinity of oxidizing char particles. Both possibilities are being investigated. The feedback from volatiles combustion is of particular interest, since volatiles flames have been observed in the TWR. Also energy feedback from volatiles flames would occur during the early stages of particle heatup (i.e. during devolatilization), where the major discrepancies in particle temperature are observed.

Energy Feedback from Volatiles Flames - Energy from volatiles combustion is fed back uniformly in PCGC-2 to all of the particles in a computational cell. This feedback occurs by convection as the volatiles react to equilibrium in the gas phase and raise its temperature. A schematic diagram of a cell with two particles is shown in Fig. III.A-2. Particle A is giving off volatiles, while particle B has not yet reached a temperature where volatile

evolution is significant (due to a different trajectory, particle size, etc.). Volatiles from particle A burn in the gas phase (if oxygen is present), raising the temperature of the gas in the entire cell. Energy feedback from this combustion is sensed in the model equally by both particles through convection. However, the energy feedback should be sensed more by particle A if the combustion is occurring more in its vicinity (i.e. if combustion is occurring in a single-particle mode). The TWR is a very lightly loaded system, and single-particle burning has been observed in photographs. Such effects would be less important in a practical reactor that is more heavily loaded and where cloud burning is the dominant mode of combustion.

In order to investigate the discrepancies between measured and predicted particle temperature in the TWR, the code was modified to model direct energy feedback from volatiles combustion. Heat of combustion data were added to the code for the light gases in FG-DVC, and an arbitrary factor was introduced for directly feeding a fraction of the volatiles heat of combustion back to the particles. The effects of including direct enthalpy feedback on the temperature and mass of a 60-μm Rosebud coal particle in an inert, uniform gas flowfield are shown in Figs. III.A-3 and 4. Including direct enthalpy feedback causes a significant increase in particle temperature (even to exceed the temperature of the gas, in the extreme case of 100 percent feedback). Particle burnout is also accelerated. However, including feedback for the more reasonable case of 50 percent feedback does not seem to result in an increase in temperature as large as what has been observed experimentally.

The moderate sensitivity of code predictions to including direct enthalpy feedback is also shown in Fig. III.A-5, where radial profiles of both measured and predicted gas and particle temperatures are shown for several axial locations. Including feedback results in hotter particles and, interestingly, less spread in particle temperature. The latter observation is quite curious, since an increase in spread in particle temperatures might be expected with selective feedback of enthalpy. However, this does not appear to be the case in Fig. III.A-5. Apparently, a fixed percentage of enthalpy feedback raises the temperature of large particles more than small particles. Such may not be the case if the fraction of feedback were calculated from a single particle model and allowed to vary.

A literature search was conducted to locate correlations or theoretical results for predicting the rate of energy feedback to a particle from a surrounding flame. Jost et al. (1983) describe a flame sheet model, which "assumes that the volatiles oxidize on a thin stoichiometric flame sheet which surrounds the coal particle. The radius of this sheet is specified when the oxygen transport to the flame equals the oxygen requirements of the escaping

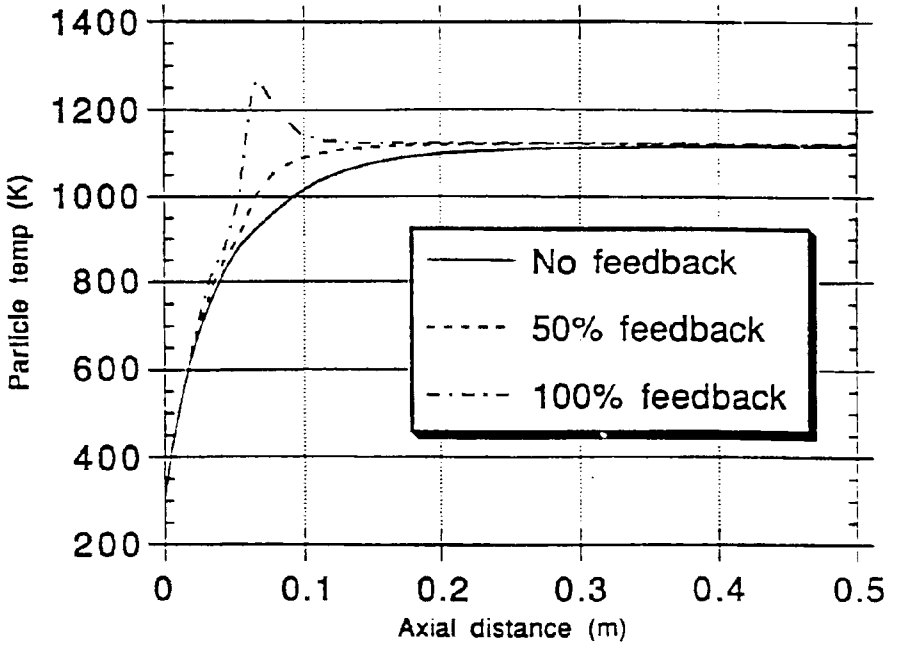

Figure III.A-3. Effect of volatiles flame enthalpy feedback on the temperature of a devolatilizing, 60-μm coal particle in a uniform, inert gas flowfield in the transparent wall reactor (Rosebud "fast" flame flow conditions)

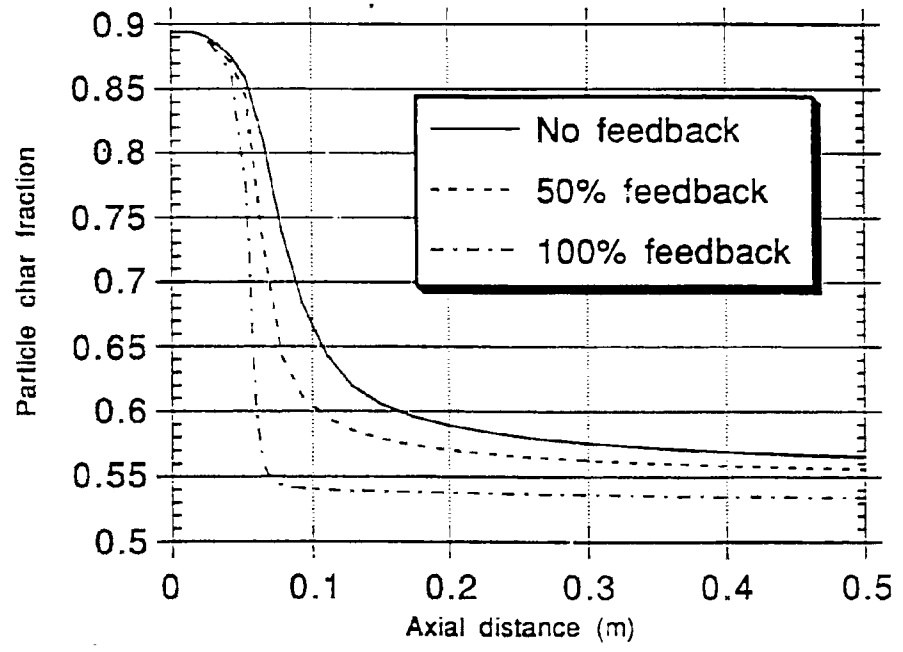

Figure III.A-4. Effect of volatiles flame enthalpy feedback on mass loss of a devolatilizing, 60-μm coal particle in an inert, uniform gas flowfield in the transparent wall reactor (Rosebud "fast" flame flow conditions)

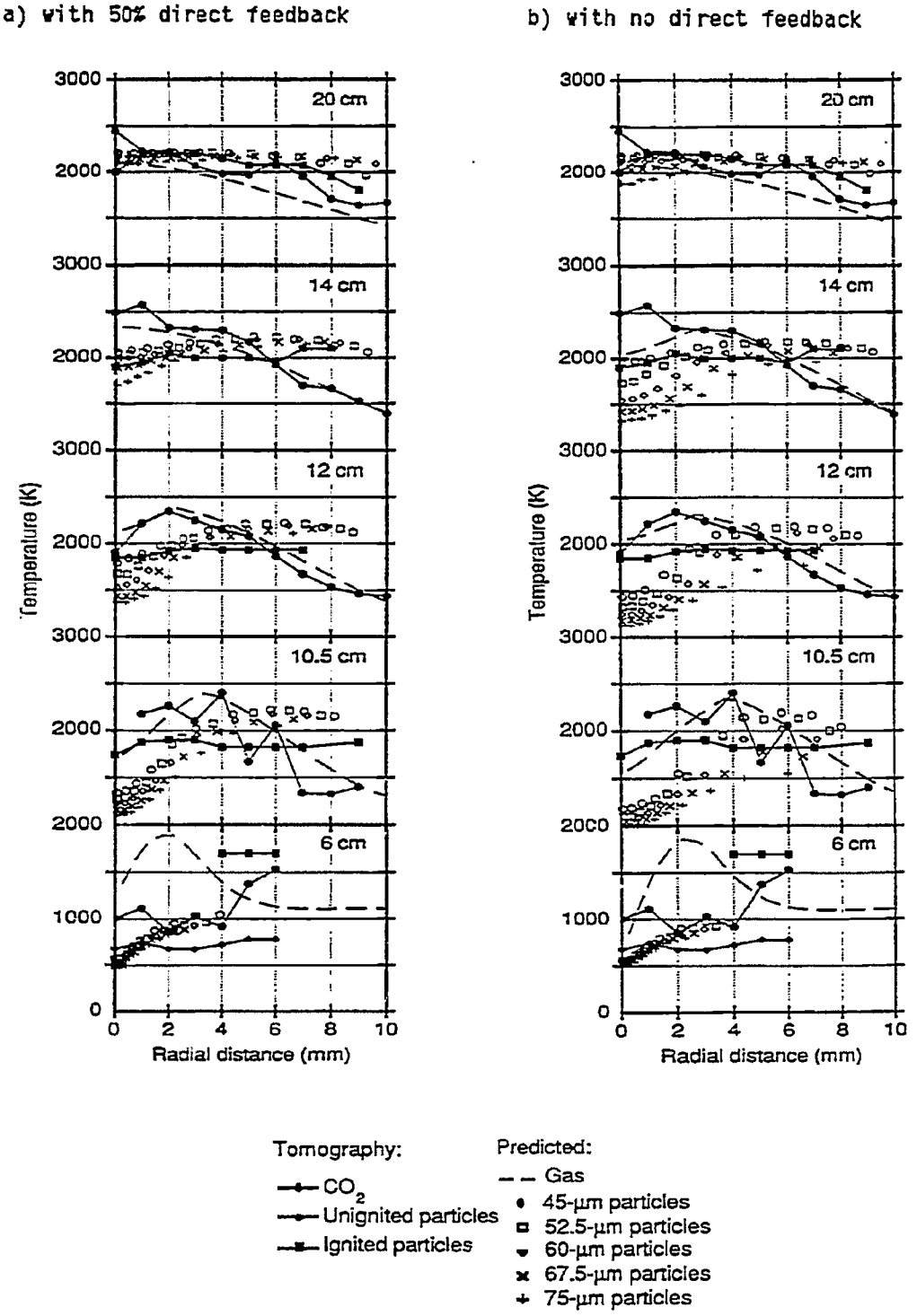

Figure III.A-5. Effect of volatiles flame enthalpy feedback on measured and predicted particle and gas temperature for combustion of Rosebud subbituminous coal ("fast" flame) in the transparent wall reactor. Measured CO_2 temperature is determined from tomographic reconstruction of line-of-sight FT-IR emission/transmission spectra.

volatiles for the combustion products assumed. The heat released during volatile oxidation is conducted both to the particle and out to the surrounding gas." Since the approach uses two algebraic equations for flame sheet radius and temperature, it is probably feasible to incorporate it into the particle submodel in PCGC-2 without too much penalty in increased computations. However, doing so is beyond the scope of this study because of the complications of interfacing with the radiation submodel. It may be possible, however, to use the approach to validate the choice of a reasonable energy feedback factor for typical combustion conditions.

Energy Feedback from Heterogeneous CO_2 Formation - In the model, when carbon oxidizes to CO_2 heterogeneously, 94.05 kcal/gmol is released at the particle surface. If CO is formed, with subsequent oxidation to CO_2 in the bulk gas, only 26.42 kcal/gmol is released at the particle surface, with the remainder (67.63 kcal/gmol) being liberated to the bulk gas which then is allowed to feed back to all particles in a computational cell. Mitchell (1989) observed that "account must be made of CO_2 formation in the vicinity" of burning char particles in order to adequately model burning rate. Employing a single-film model of a burning carbon sphere with a fraction ψ of the carbon being converted to CO_2 at the particle surface, he was able to adequately describe the burning behavior of coal char particles in the 75 to 125 μm size-range. Applying this model to char particles of bituminous coals, he found that "as much as 15% of the carbon content of the particle can be converted to CO_2 at temperatures in the range 1600 to 1700 K. At temperatures above 1800 K, CO is essentially the sole heterogeneous reaction product."

The effect of heterogeneous CO_2 formation on temperature and reaction rate of a 60-μm carbon particle at the conditions of the Rosebud "fast" flame in the TWR was investigated by varying the fraction of CO_2 formed (ψ) between zero and unity. The kinetic parameters of Goetz et al. (1982) for a subbituminous C coal char were used in this study. Results are shown in Fig. III.A-6. The differences between the "all-CO_2" ($\psi = 1.0$) and "all-CO" ($\psi = 0.0$) predictions are quite significant. When CO_2 is the product, the maximum particle temperature is 3500 K (radiation was not included in this calculation and heat loss was limited), whereas it is only 2500 K when CO is the product. Interestingly, the particle burns out more slowly when CO_2 is the product, even though the temperature is higher. The reason for this difference can be seen by looking at the oxidation rate and resistances. The rate is much higher in the case of CO production. The higher rate is due to a lower resistance to mass transfer, which is controlling at high particle temperature, since only one oxygen atom is required per carbon atom rather than two. The effect of 15

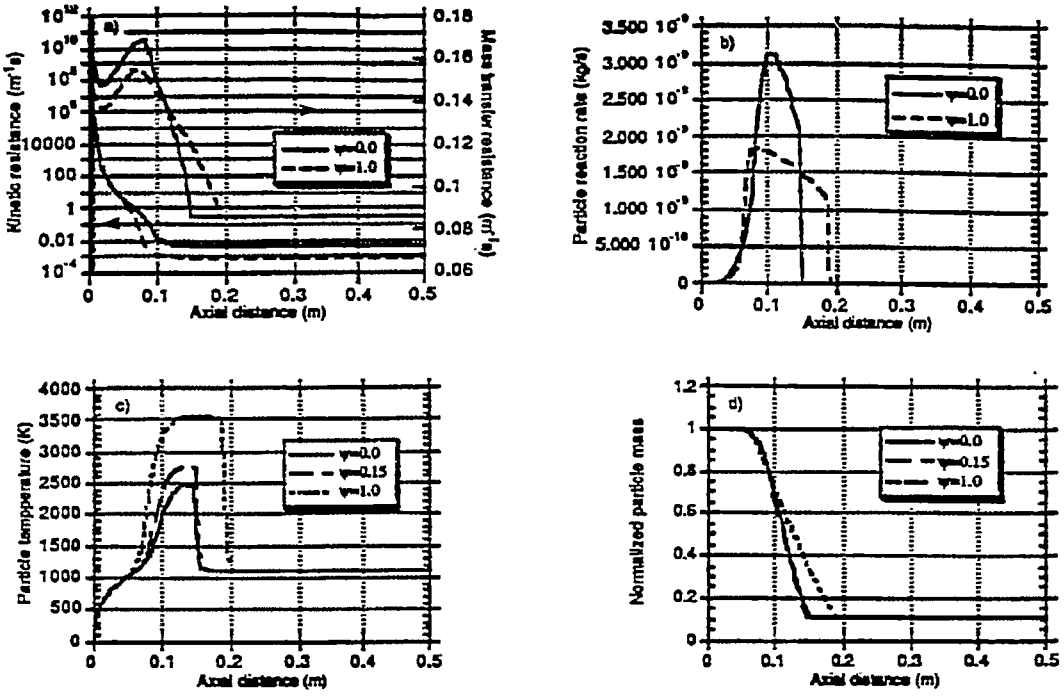

Figure III.A-6. Effect of heterogeneous CO_2 formation (Ψ = CO_2 formed/total C reacted) on a) oxidation rate resistances, b) oxidation rates, c) mass loss, and d) temperature of a 60 μm carbon particle in a uniform gas flowfield in the transparent wall reactor (Rosebud "fast" flame flow conditions). Radiation effects were neglected.

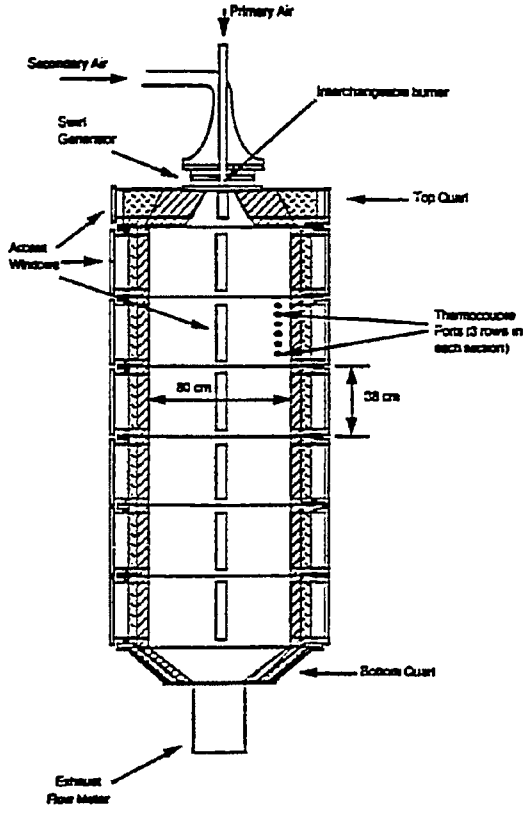

Figure III.A-7. Cross-sectional diagram of the BYU-ACERC controlled-profile reactor.

percent CO_2 formation (Mitchell, 1989) on temperature is on the order of 200 K, and the effect on mass loss is negligible.

BYU/ACERC Controlled-Profile Reactor (CPR) - Simulations were performed for a natural gas flame in the CPR. A diagram of the reactor is shown in Fig. III.A-7. Input data are shown in Table III.A-1. The reactor is referred to as "controlled-profile" because of its computer-controlled wall temperature profile. Using the reactor's access windows, gas temperature, composition, and three velocity components were measured with independent funding in a swirling natural gas flame (Eatough, 1991). Gas temperature, measured with a suction pyrometer, is compared with code predictions in Fig. III.A-8. The potential effect of soot on radiation was investigated theoretically by injecting carbon particles of 1 μm diameter with the primary gas. A loading of 0.1 lb solids/lb gas was assumed. The effect of radiation model type was also investigated.

The effect of radiation model type was insignificant, except at large axial distances. Both models underpredicted the gas temperature at the outlet, with the underprediction by the flux model being more significant. Only the particle-free simulations underpredicted the temperature. The predicted outlet temperature with injected carbon particles was 1375 K.

Particle trajectories for the particle-laden case are shown in Fig. III.A-9. The 1-μm particles were injected at 10 starting locations in the primary duct. The presence of the particles causes smoother radial temperature profiles. The gas is hotter than otherwise predicted near the centerline and near the wall. The shape of the predicted profile agrees much better with the shape of the measured data at axial locations of 0.26, 0.31, 0.36, 0.46, 0.66, and 0.76 m. The effect of the particles, which were considered inert, is thought to occur primarily through radiation. Particles in cold areas of the reactor receive radiation and act as heat sources to the gas. Particles in hot areas radiate heat away and act as heat sinks. These effects can be seen in the comparisons in Fig. III.A-8. In general, however, the predicted temperature is too high.

Other predictions and data for the particle-free case are shown in Figs. III.A-10 through 13. The predicted radial profiles of axial velocity agree well with the measured profiles. Predicted radial velocity agrees more closely with data at locations farther away from the inlet than close to the inlet, as does also temperature. The predicted CO_2 concentration near the inlet agrees more closely with the data than O_2 concentration at the same location. Both the

Table III.A-1. PCGC-2 input data for simulation of natural gas combustion in the CPR.

GEOMETRY		
Primary tube ID	0.02664 m	
Secondary tube ID	0.0984 m	
Chamber ID	0.80 m	
Chamber length	2.65 m	
Primary wall thickness	0.00353 m	
Quarl half-angle	35.0 degrees	
Quarl Length	0.20 m	
MASS FLOW RATES		
Primary gas	0.002611 kg/s	
Secondary gas	0.047252 kg/s	
GAS PROPERTIES	Primary	Secondary
Temperature (K)	298.0	298.0
Pressure (KPa)	86.0	86.0
Swirl number	0.0	1.45
GAS COMPOSITION (mass fraction- dry basis)	Primary	Secondary
CO_2	0.016252	0.00000
CH_4	0.800761	0.000000
C_2H_6	0.120040	0.00000
C_3H_8	0.054172	0.00000
N_2	0.008775	0.76700
O_2	0.000000	0.23300

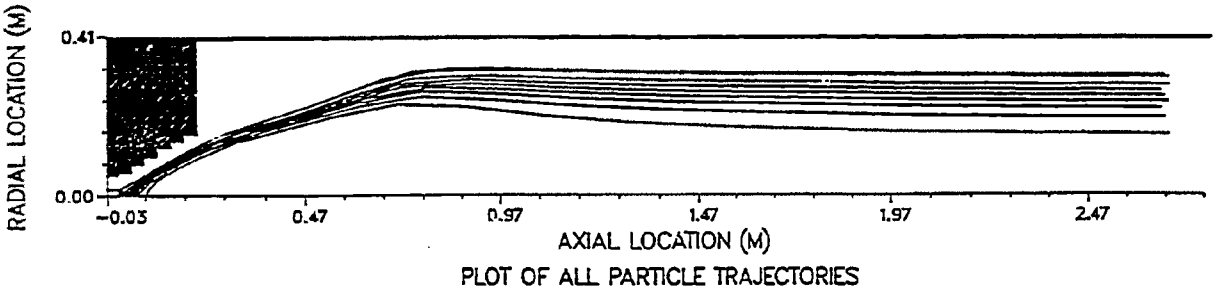

Figure III.A-9. Predicted particle trajectories for simulation of soot radiation effects in a natural gas flame in the CPR.

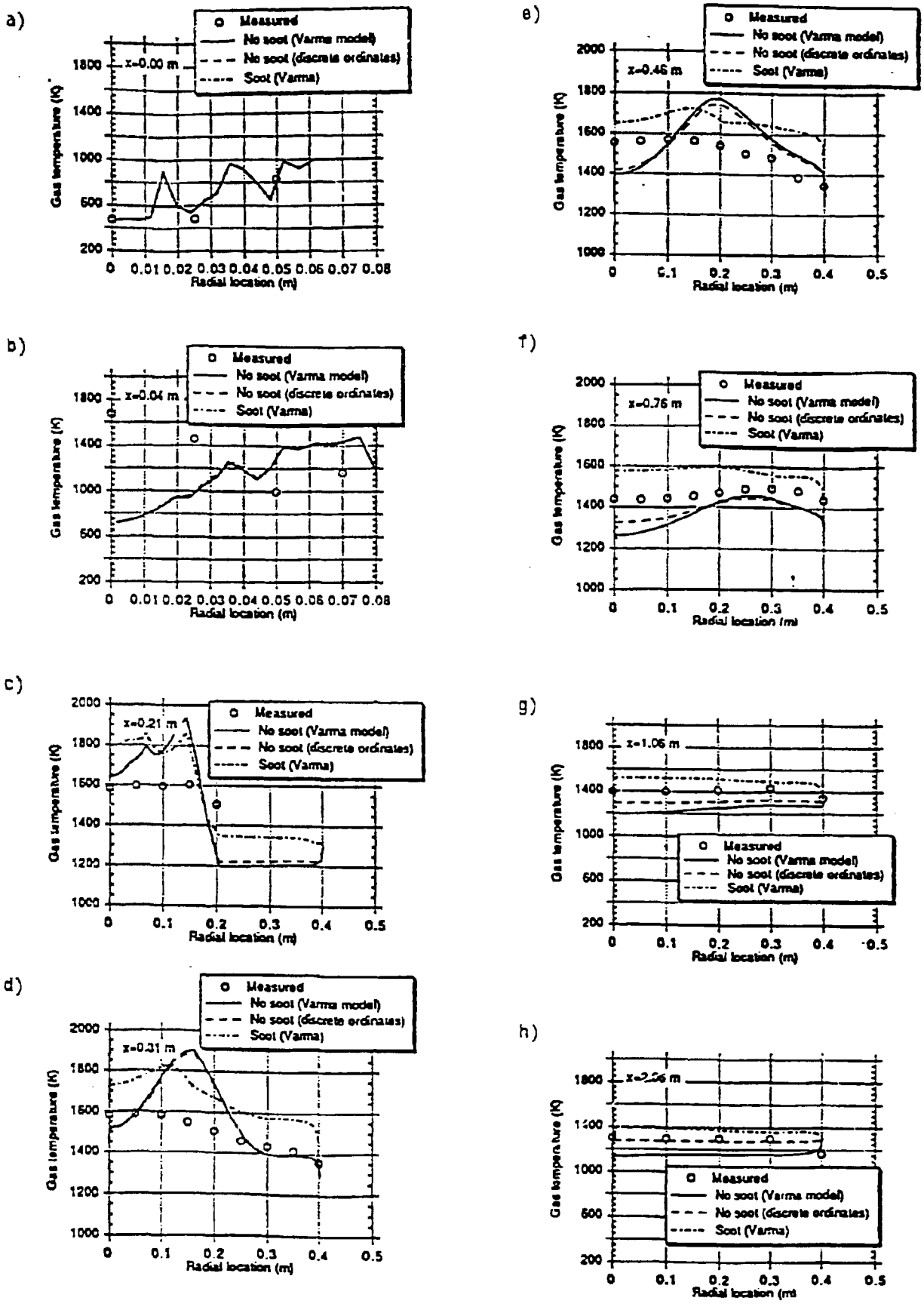

Figure III.A-8. Predicted gas temperature compared with experimental data (Eatough, 1991) for a natural gas flame in the CPR. Varma six-flux (Varma, 1979; Varma and Pratt, 1978) and discrete ordinates radiation models were used.

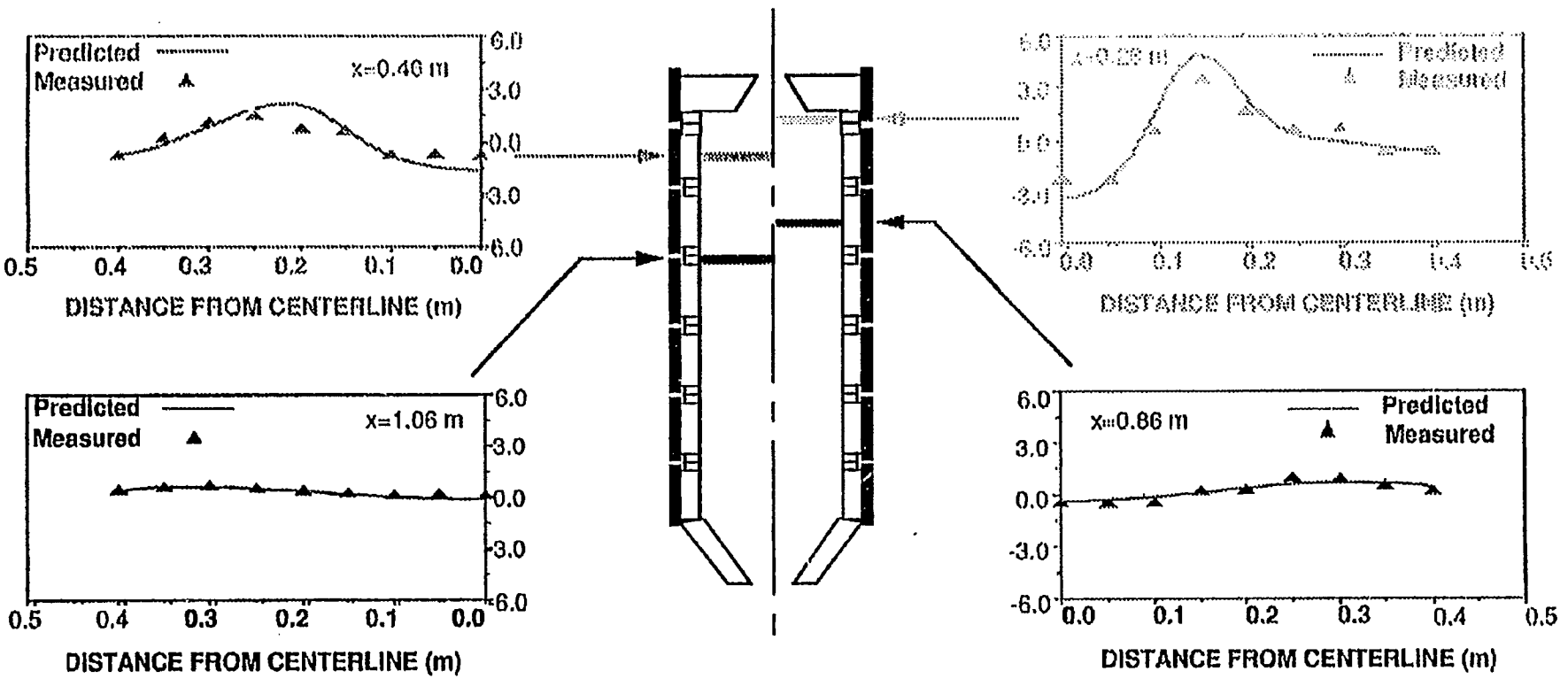

Figure III.A-10. Predicted and measured axial velocity for a natural gas flame in the CPR.

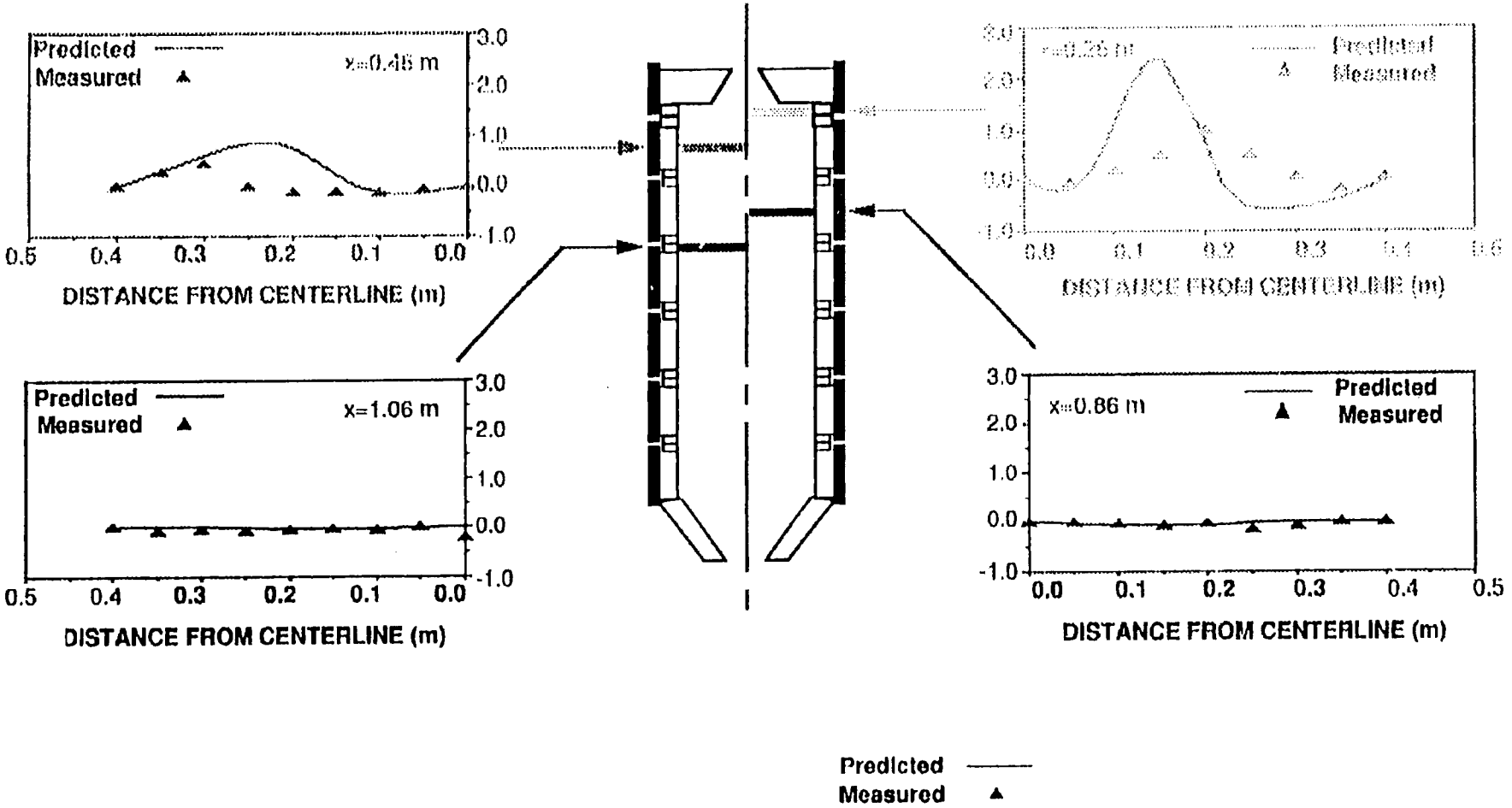

Figure III.A-11. Predicted and measured radial velocity for a natural gas flame in the CPR.

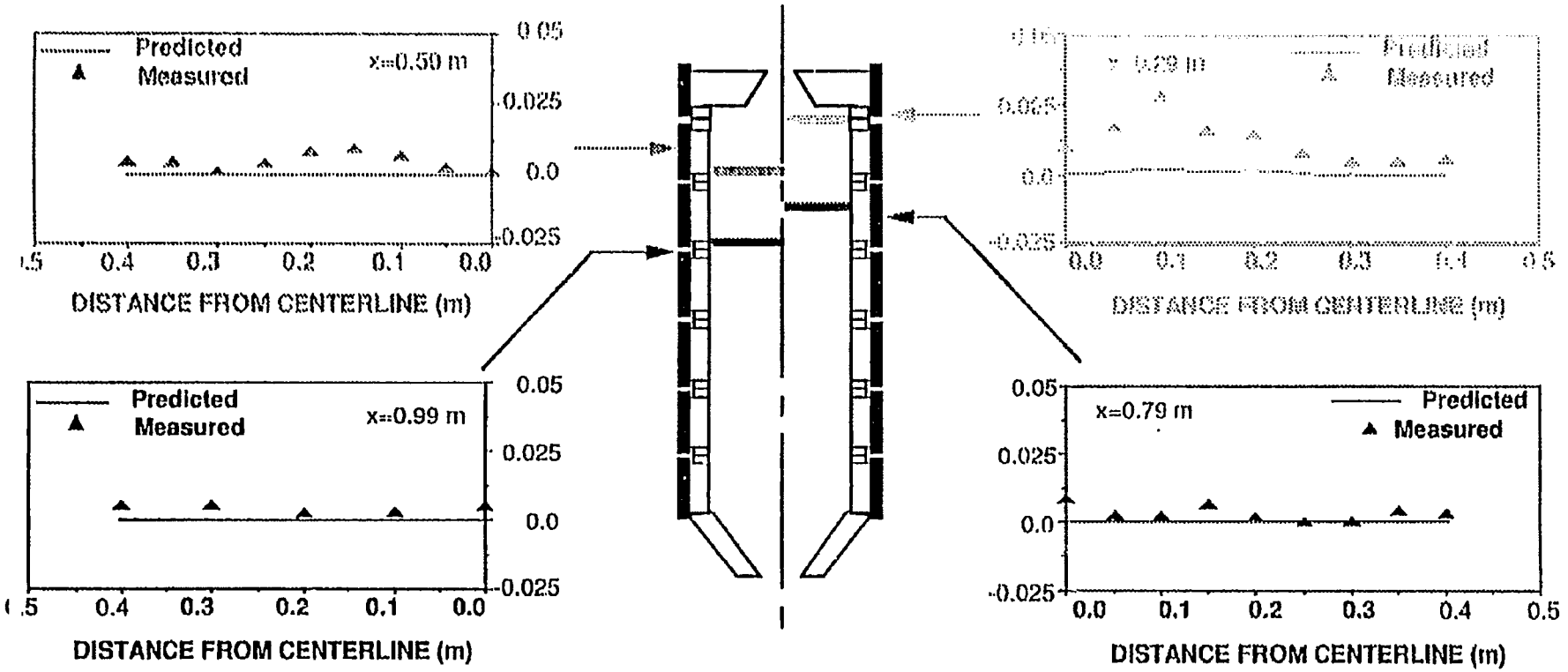

Figure III.A-12. Predicted and measured O_2 concentration for a natural gas flame in the CPR.

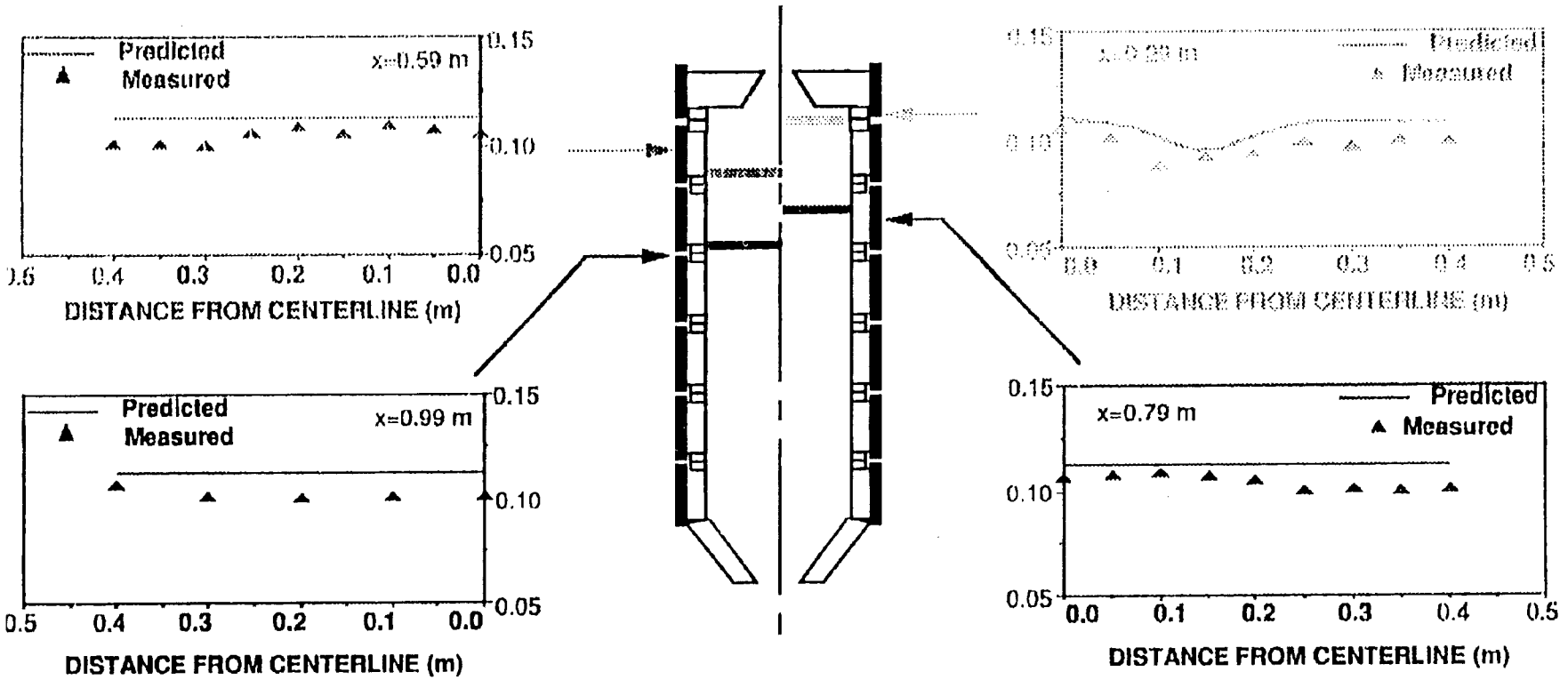

Figure III.A-13. Predicted and measured CO_2 concentration for a natural gas flame in the CPR.

external (counter-clockwise) and internal (clockwise) recirculation zones are visible in the velocity vector plot (not shown).

Imperial College Reactor - Costa et al. (1990) reported gas phase composition, temperature, and char burnout for two swirl numbers in the axisymmetric, Imperial College reactor. The near-field measurements of ignition distance (Lockwood et al., 1980, 1984; Lockwood and Salooja, 1983; Lockwood and Mahmud, 1988) are significantly underpredicted by the Imperial College 2-D model. The quality of the data appears to be quite good, e.g. the radial oxygen concentration profiles are quite symmetric around the centerline. Since one of the potential benefits of detailed coal chemistry submodeling is more accurate prediction of particle ignition, these data are of significant interest to this study.

Six data sets were requested and received from Imperial College, as summarized in Table III.A-2A. Two different coals were used, namely, low-volatile UK Oakdale and high-volatile UK Geddling coals. All six cases have been modeled using the base 2-D code (without FG-DVC). Difficulty was initially experienced in converging the cases because of energy coupling between gas and particles through radiation. Convergence was achieved only after under-relaxing the radiation source terms in the gas enthalpy equation. Figure III.A-14 shows the velocity vector, burnout, and particle trajectory plots for Case A. The direction of both the internal and external recirculation zones is opposite to what it should be. Because of this flow pattern, the particles are thrown to the wall, resulting in a higher residence time at axial locations near the inlet. This results in particle burnout very early in the reactor. The radial profiles of all species are therefore constant after a short distance from the inlet. Effort is being made to detect the source of the problem.

BYU Gasifier - Four cases of coal gasification in the BYU gasifier (Azuhata et al., 1986) were simulated with the PCGC-2 base code (without FG-DVC) as shown in Table III.A-2B. Results of North Dakota lignite gasification are presented in this report. The single-step rate of Solomon et al. (1986) was again used for devolatilization in the base code. However, a volatiles fraction of 0.7 was used instead of 0.4 to match experimental burnout. Volatiles fraction during devolatilization is a function of final temperature (Smoot and Smith, 1985). Solomon et al. went to a maximum final temperature of about 1100 K. For typical coal combustor temperatures (e.g. 2100 K), the volatiles yield may be above 60 percent (Smoot and Smith, 1985). Since gasifier temperatures may reach above 2500 K, a volatile fraction of 0.7 is not unreasonable for the present simulation.

Table III.A-2 PCGC-2 evaluation cases for coal combustion and gasification in the Imperial College combustor and BYU gasifier.

A. Coal Combustion (Imperial College) [Costa, et. al., (1990)]

Case #	Coal type	Diameters (m)			Chamber length (m)	Mass flow rates (kg/s)			Swirl number	
		Pri.	Sec.	Cham.		Pri.	Sec.	Solids	Pri.	Sec.
Trial A	UK Geddling	.0222	.056	.60	3.0	.00785	.02872	.00305	0	0.78
Trial B	UK Geddling	.0222	.056	.60	3.0	.00785	.02872	.00305	0	1.03
Trial C	UK Geddling	.0222	.056	.60	3.0	.00806	.02958	.00344	0	1.45
Trial D	UK Geddling	.0222	.056	.60	3.0	.01075	.03942	.00456	0	1.03
Trial E	UK Geddling	.0222	.056	.60	3.0	.01075	.03942	.00456	0	1.45
Trial F	UK Oakdale	.0222	.056	.60	3.0	.01067	.03886	.00400	0	1.45

B. Coal Gasification (BYU) [Soelberg (1983), Brown (1984)]

Case #	Coal type	Diameters (m)			Chamber length (m)	Mass flow rates (kg/s)			Swirl number	
		Pri.	Sec.	Cham.		Pri.	Sec.	Solids	Pri	Sec.
Soelberg	Utah bituminous	.0131	.0287	.20	1.19	.0073	.0018	.0066	0	0
Brown 1	Wyoming subbituminous	.0131	.0287	.20	2.0	.0066	0.0	.00616	0	0
Brown 2	N. D. lignite	.0131	.0287	.20	2.0	.00774	0.0	.00776	0	0
Brown 3	Illinois #6 bituminous	.0131	.0287	.20	2.0	.0092	.000667	.00822	0	0

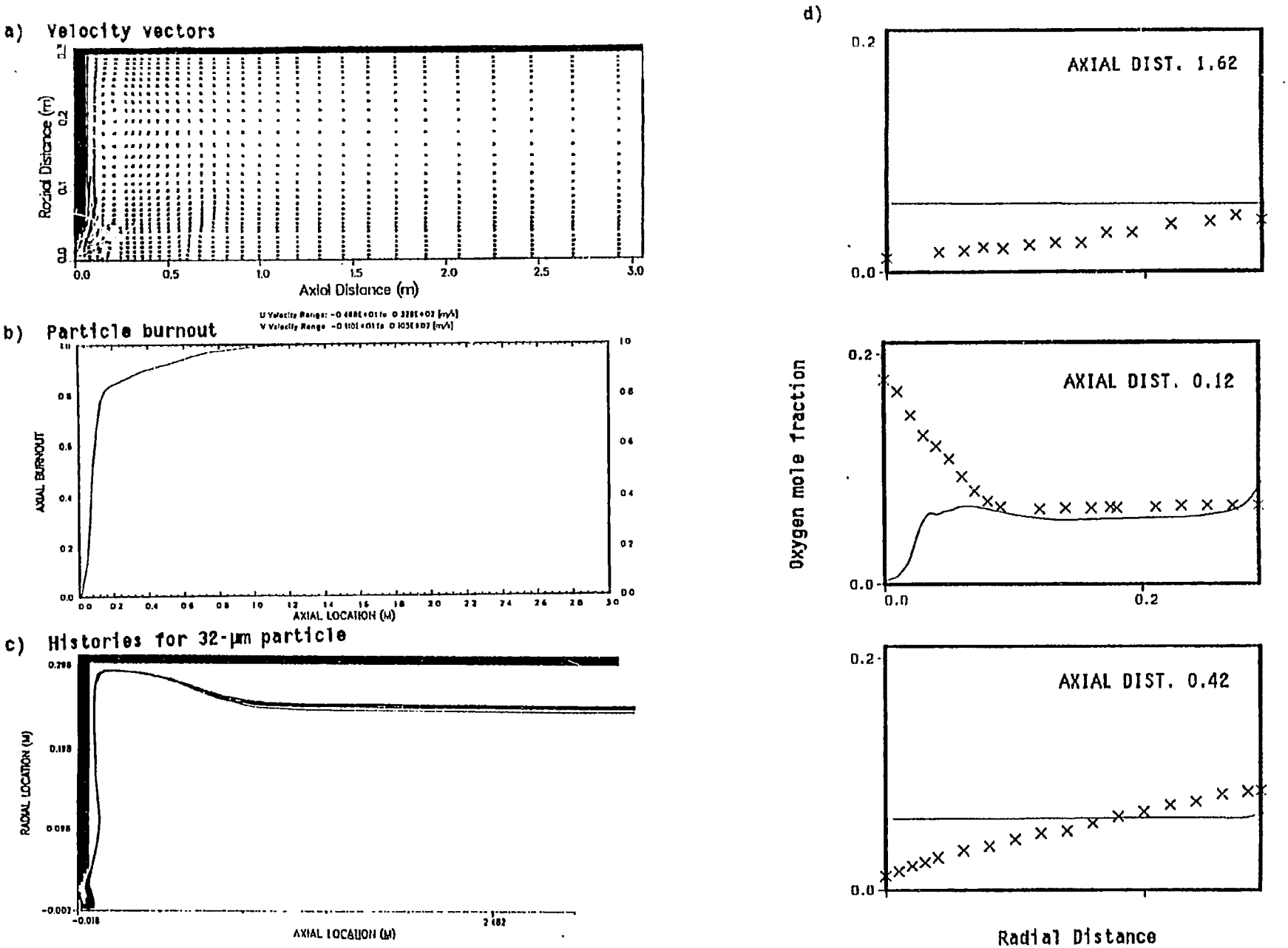

Figure III.A-14. Prediction for coal combustion (Case A in Table III.A-2A) in the Imperial College Combustor.

Figure III.A-15a shows the velocity vect r plot, where the external recirculation zone can be distinctly identified. It is also to be noted that there is no internal recirculation zone, which is expected from a non-swirling flow. Figure III.A-15b shows the burnout of coal along the length of the reactor. Burnout at the exit is predicted to be about 79 percent which agrees with the experimental value of 80 percent. Figure III.A-15c shows the axial particle history of a single particle of 32 μm diameter. Devolatilization is very rapid and finishes almost at the start of the reactor, followed by a very slow char oxidation process. This slow char oxidation is due to a high particle loading, low temperature, and low O_2 concentration. Figure III.A-16 shows forward and aft radial profiles of H_2, CO, CO_2, and O_2. The predicted profiles of H_2 and CO_2 match nicely with the experimental profiles, especially at the exit of the reactor. Near-burner predictions of H_2 and CO are higher while CO_2 profiles are slightly underpredicted. The predicted profile of O_2 shows that oxygen is depleted very early in the reactor.

Sensitivity to Particle Optical Properties - The sensitivity of the above calculations to particle optical properties was investigated by performing simulations using two sets of absorption and scattering coefficients as shown in Table III.A-3. In both cases, the particle size distribution was flat. One set of coefficients was obtained from the user's manual and the other was obtained from AFR based on Mie theory calculations using measured particle properties. The coal-gas mixture fraction was slightly higher when the AFR values were used, but the differences in particle burnout, particle temperature, and gas temperature were insignificant. These results are in concurrence with the findings of Jamaluddin and Smith (1986), who also showed that PCGC-2 predictions are insensitive to particle optical properties.

Correlations were developed for the code to predict absorption and scattering coefficients as a function of particle size. These correlations eliminate the need for the user to specify particle optical properties in the input data. The correlations are based on Mie theory calculations. Figure III.A-17 shows Mie theory predictions (solid lines) of coefficients of extinction, scattering, and absorption as functions of the particle size parameter $\pi d_j/\lambda$, where λ is the wavelength (here assumed to be 2 μm). The dashed lines are values reported in the user's manual, also obtained from Mie theory calculations. The reason for the difference between the two sets of calculations is not known, since both were based on Mie theory. However, the difference is fairly small and, since the code predictions are insensitive to particle optical properties, will be neglected. The correlations used in PCGC-2 are based on the more recent Mie theory calculations, since the program used to obtain the original values is not available for further comparison.

a) Velocity Vectors

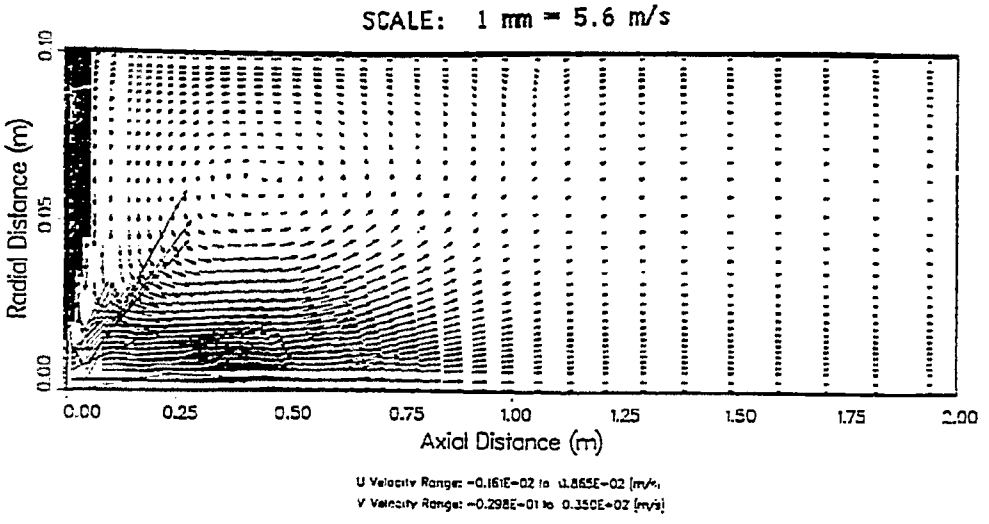

b) Particle burnout

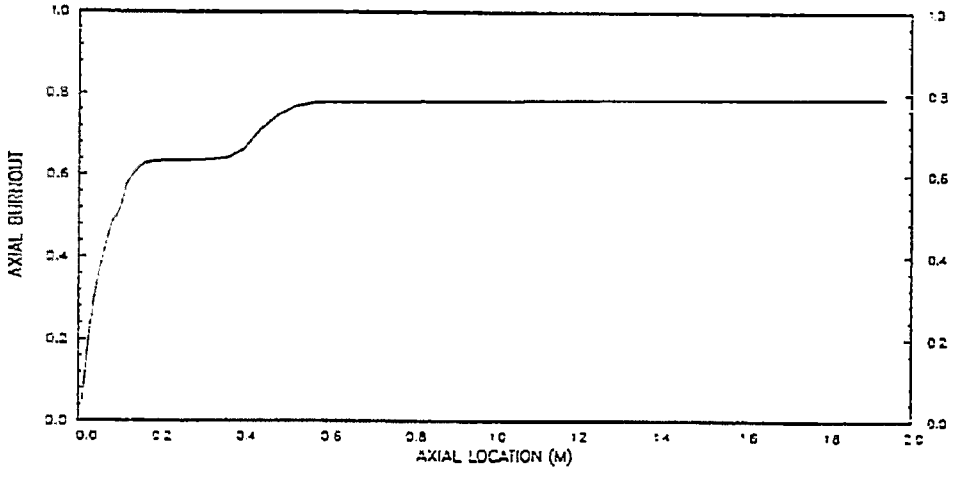

c) Histories for 32-μm particle

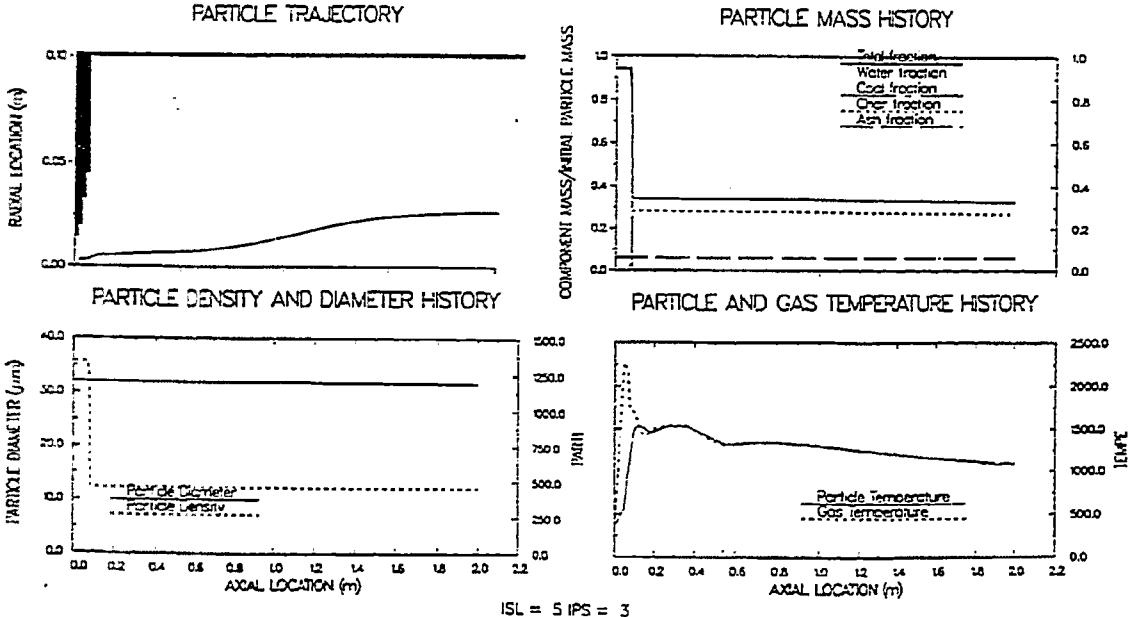

ISL = 5 IPS = 3

Figure III.A-15. Predictions for gasification of North Dakota lignite in the BYU gasifier.

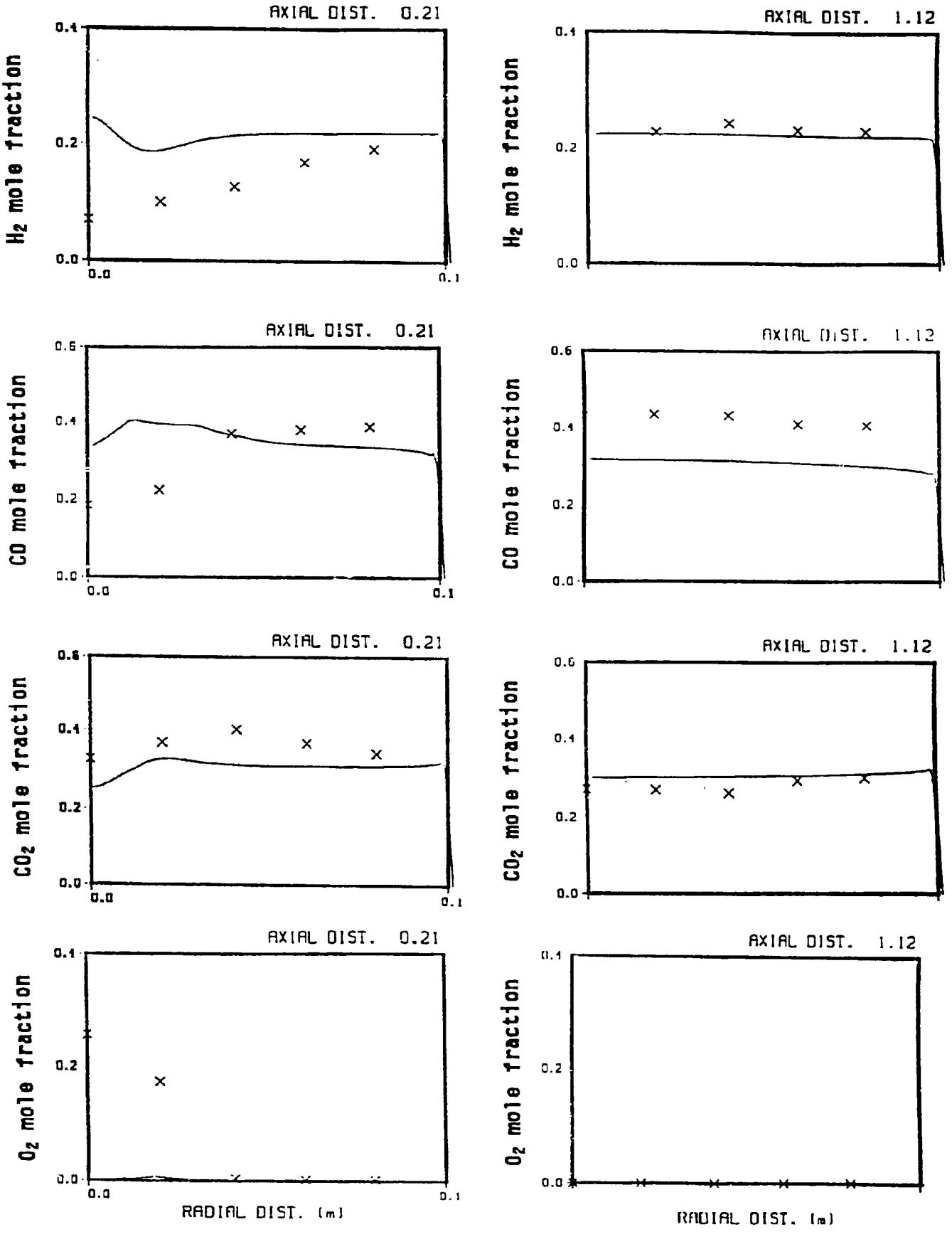

Figure III.A-16. Predicted and measured gas concentration for gasification of atmospheric lignite in the BYU laboratory-scale gasifier at atmospheric pressure. O_2/coal ratio: 0.93 kg/kg. Data are from Brown (1985). Predictions are by base version of PCGC-2.

Table III. A-3

OPTICAL PROPERTIES FOR NORTH DAKOTA LIGNITE PARTICLES USED IN SENSITIVITY STUDY

Particle diameter (μm)	From User's Manual (2μm wavelength and refractive index of 1.93[1-i(0.53)])		From AFR (averaged over 1.5 - 10 μm and using experimentally measured refractive index)	
	Absorption coefficient	Scattering coefficient	Absorption coefficient	Scattering coefficient
20	0.88	0.35	0.80	0.46
40	0.85	0.33	0.89	0.28
60	0.83	0.32	0.91	0.21
80	0.81	0.30	0.92	0.21
100	0.80	0.30	0.90	0.19

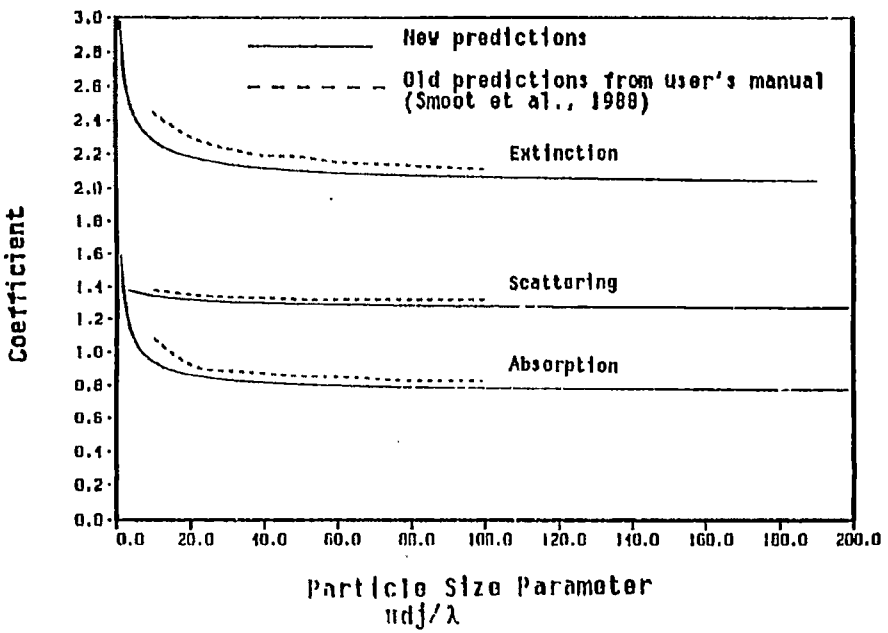

Figure III.A-17. Particle radiation properties predicted by Mie theory at a wavelength of 2μm and refractive index of 1.93(1-i(0.53)).

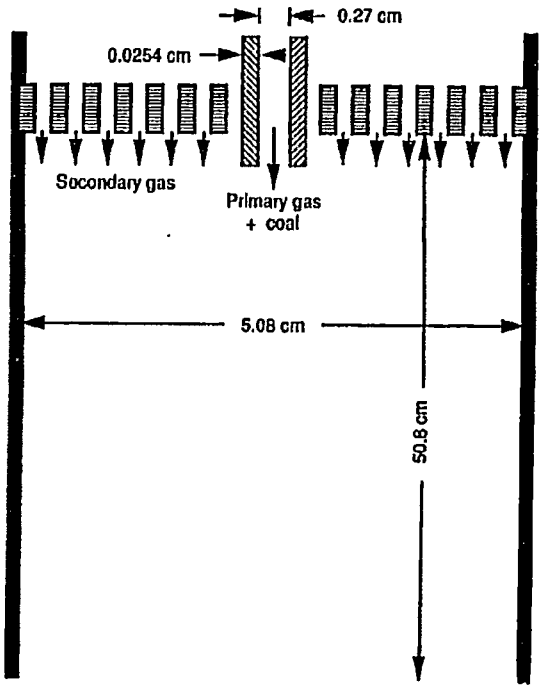

Figure III.A-18. ABB CE drop-tube facility.

ABB Combustion Engineering (CE) Reactor - Eight cases of coal and char combustion in the ABB CE drop-tube furnace were simulated. Two different high-volatile, bituminous coals, namely U.S. McCall and South African coals, were used. Cases were also simulated with chars of the above-mentioned coals. The flow conditions were assumed to be laminar. Solomon et al.'s (1986) one-step model was used for devolatilization. Combustion Engineering Inc. supplied the parameters for char oxidation kinetics.

A schematic of the ABB CE drop-tube furnace is shown in Fig. III.A-18. Primary gas and coal flow downward through a 0.27-cm-diameter duct. Secondary gas flows through a flow straightener with 151 holes. The diameter and length of the reactor are as shown.

Table III.A-4 shows measured and predicted values of gas composition at the exit along with the primary and secondary gases used in each case. Only the exit values are compared since they are the only experimental values supplied. DeSoete's kinetics (1975) were used for fuel NO in the pollutant calculations, and the extended Zel'dovich mechanism was used for thermal NO. Levy et al.'s (1981) global decay expression was used for char/NO decay calculations.

The predicted and measured values of oxygen concentration at the exit are in quite good agreement. For coal combustion, the predicted CO concentration is found to be in good agreement when there is argon in the secondary gas. If there is air in the secondary flow, the predicted values are found to be substantially lower than the measured values. Similar trends in the predicted values were observed for cases with char oxidation. The measured values of CO concentration at the tube exit are found to have some inconsistencies.

The maximum error in the predicted values of NO concentration is found to less than 52 percent. The predictions are always lower than the measured values except for char combustion cases with O_2 and Ar in the secondary. But in general, the predicted trends are similar to those observed during experiments.

Goudey furnace - Simulations were performed under independent funding for the near-burner field of the NYSEG Goudey plant. The plant is located at Johnson City, New York. A schematic of the furnace is shown in Fig. III.A-19. Near-burner measurements were taken at Level 2, following the probe paths shown in Fig. III.A-19b and 20b. The data were compared with PCGC-2 predictions, assuming the axis of symmetry coincides with the centerline of the burner jet. As shown in the figure, the furnace is corner-fired, and the centerline is offset from the 45-degree diagonal by 4 degrees and tilted downward. The equations for coordinate transformation from the Goudey reactor coordinates to

Table III.A-4: PCGC-2 predicted values of NO_x, CO and O_2 against measured values

Case No.[a]	Coal type	Coal/ Char	Secondary gas	Species	Measured value		PCGC-2 prediction	
dtfs1	US McCall	coal	Air	NO_x	133	ppm	93	ppm
				CO	70	ppm	22	ppm
				O_2	20	%	20	%
dtfs2	US McCall	coal	21% O_2 79% AR	NO_x	90	ppm	71	ppm
				CO	58	ppm	61	ppm
				O_2	20	%	20	%
dtfs3	US McCall	char	21% O_2 79% AR	NO_x	45	ppm	68	ppm
				CO	13	ppm	62	ppm
				O_2	19	%	20	%
dtfs4	US McCall	char	Air	NO_x	116	ppm	108	ppm
				CO	38	ppm	25	ppm
				O_2	19	%	20	%
dtfs5	South African	coal	Air	NO_x	128	ppm	92	ppm
				CO	52	ppm	22	ppm
				O_2	20	%	20	%
dtfs6	South African	coal	21% O_2 79% AR	NO_x	85	ppm	68	ppm
				CO	50	ppm	62	ppm
				O_2	20	%	20	%
dtfs7	South African	char	Air	NO_x	107	ppm	95	ppm
				CO	74	ppm	24	ppm
				O_2	19	%	20	%
dtfs8	South African	char	21% O_2 79% AR	NO_x	45	ppm	68	ppm
				CO	79	ppm	62	ppm
				O_2	19	%	20	%

[a] dtfs = drop tube facility system

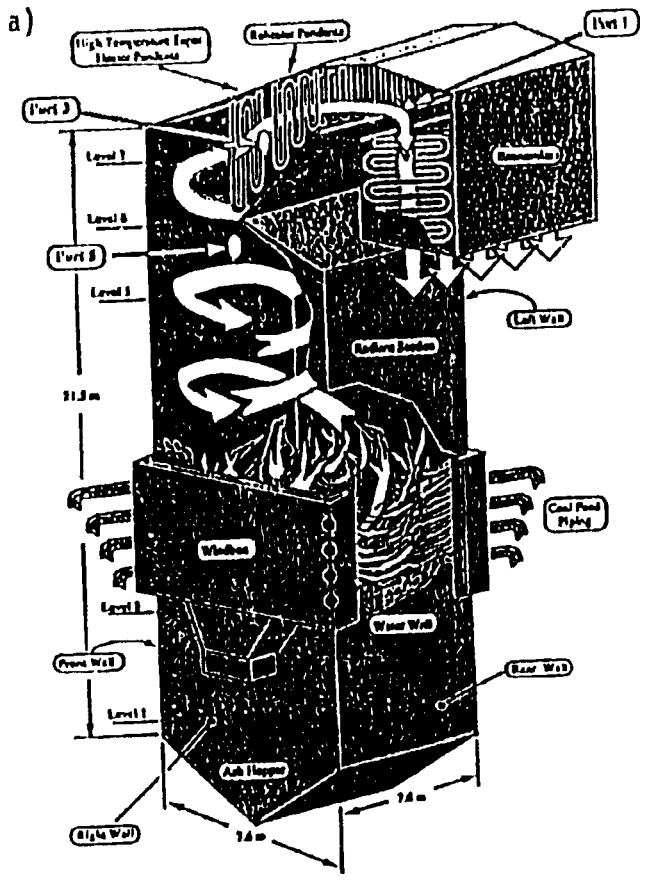

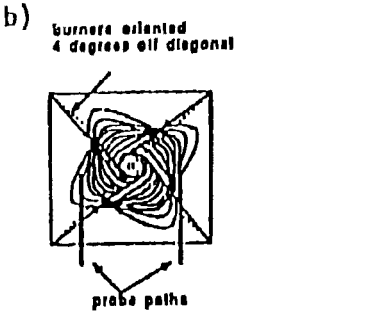

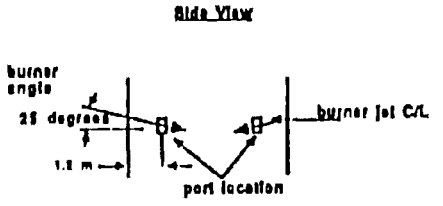

Figure 6D-3. Schematic of Goudey Station Configuration

Figure III.A-19. Schematic of the Goudey NYSEG combustor (taken from Cannon et al., 1991).

the axisymmetric coordinate system with axis corresponding to the burner centerline and origin corresponding to the burner inlet are given in the appendix.

A plot of the predicted particle trajectories and assumed geometry for the simulation is shown in Fig. III.A-20a. The angle between the reactor wall and burner centerline was assumed to be 45 degrees (i.e. the 4-degree offset was neglected). After a distance equal to half the width of the reactor, the wall was assumed to converge back toward the reactor centerline, in order to prevent recirculation at the exit plane and achieve convergence over a relatively short axial length. Otherwise, the reactor length would need to be increased by a factor of 3 or more in order to provide enough distance so as to not have any recirculation at the reactor exit plane. The code does not converge if there is recirculation at the reactor exit plane. Since it is only the near-burner region of the calculation that is of interest, the modified geometry to achieve convergence for a shorter total axial distance of simulation was assumed to have no adverse effect. In fact, it was necessary to allow for more detailed simulation of the near-burner region with the same number of total grid points.

A contour plot of predicted temperature is shown in Fig. III.A-20b. The probe paths with measurement locations is also shown. Temperature was measured at most, but not all, of the indicated locations. Due to the uncertainty in the burner tilt angle, two values were tried. Oxygen concentration and gas temperature are shown in Figs. III.A-20c and 20d, respectively. The curves represent a least-squares fit of the experimental data. The horizontal axis is the distance from the wall. The predicted temperature rise and oxygen decrease with increasing distance from the wall agree well with the experimental data at distances less than 1.5 m. The disagreement at 1.5-2 m may be due to 3-dimensional effects in the furnace.

The applicability of PCGC-2 to this 3-D configuration, even in the near-burner region, is questionable. Subsequent predictions will be made with a 3-D code under independent funding.

User-Friendliness and Robustness

Improving code user-friendliness and robustness is an on-going activity. During the last year, work continued on simplifying code input, developing a graphical user interface, improving code diagnostics, and developing a graphical post-processor.

Code input - User-friendliness was improved during the last year by adding a sorting algorithm for Lennard-Jones parameters supplied in the input

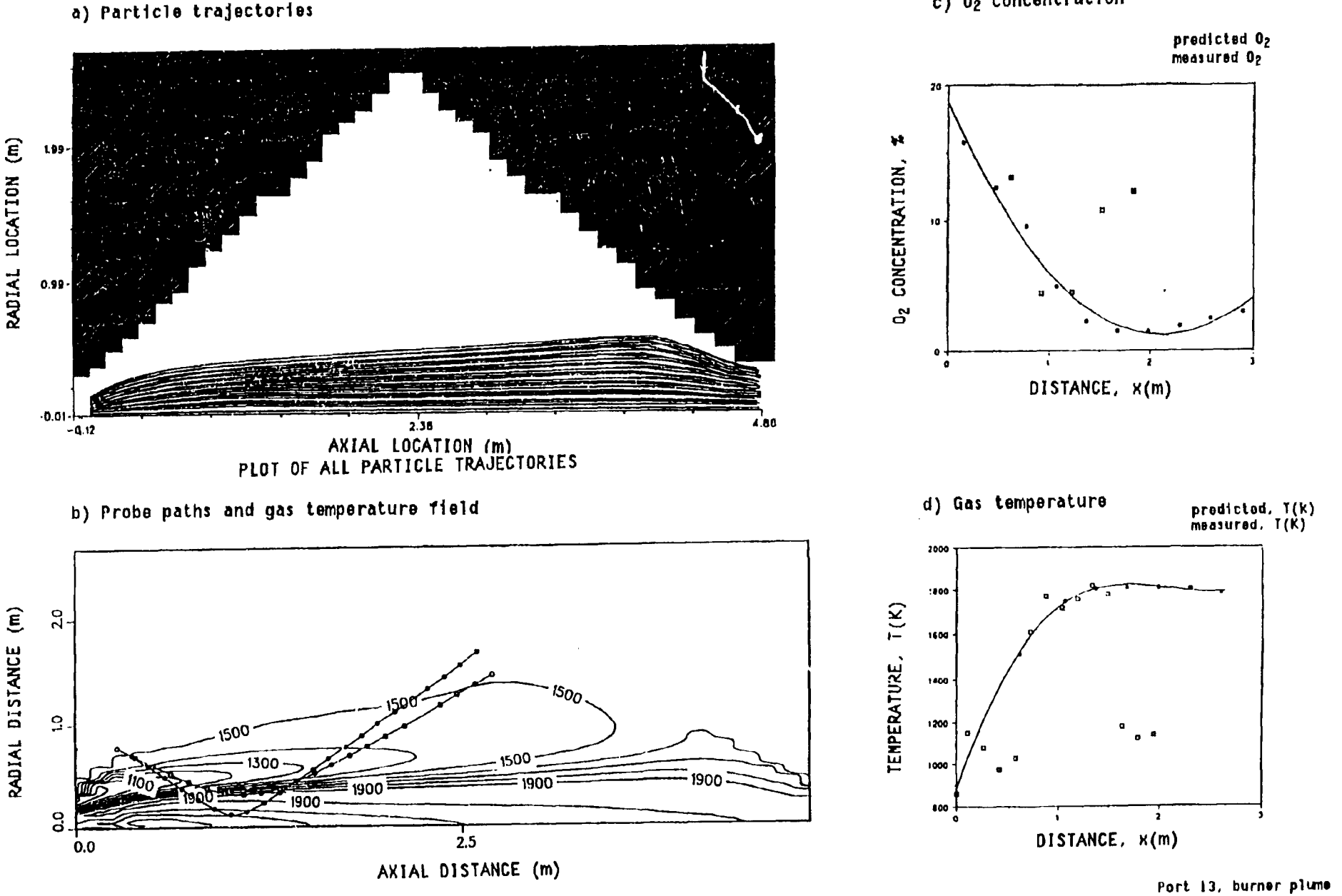

Port 13, burner plume
AFT 2300K
-24 degree burner tilt
700K wall temperature

Figure III.A-20. Predictions and data for Goudey furnace.

file for thermodynamic data. These data have often been a source of input errors for the inexperienced user, because they were required for each gas species and in the same order as the other data for the species. Now the order in which they can be supplied is arbitrary, and the program will issue a warning if any required data are missing. Also, correlations were developed as explained earlier for particle optical properties as a function of particle size to eliminate the need for the user to specify particle optical properties in the input data.

Graphical Interface - A graphical user interface (GUI) for preparing code input was extended to include particle combustion data. The GUI runs under the OPEN LOOK™ windowing system developed by Sun Microsystems and available on Sun workstations. The particle data window is shown in Fig. III.A-21. The top part of the window contains logical variables which toggle between their true and false states by clicking the mouse on the arrow. A brief text string by the side of the arrow explains the meaning of the current setting. Below the logical variables are numeric fields for specifying the number of trajectories, particle sizes, etc. These values are changed by using the mouse to position the cursor in the appropriate numeric field and entering the data from the keyboard. Directly below the numeric field for specifying the maximum number of particle iterations for convergence is a stack button for selecting the option for interpolating gas properties. Again, the user can cycle through the available options by clicking the mouse on the box with the arrow. Below the stack button for the gas properties interpolation index is an array of numeric fields for specifying the particle diameters. A stack button for cycling through available unit options is also provided. At the bottom of the window, numeric fields are provided for specifying particle properties. Stack buttons allow the user to select from several unit options.

Code Diagnostics - Diagnostic messages have continually been added to the code when problems with code input have occurred. These messages will assist in detecting errors in code input in the future. During the past year for example, a problem was encountered in the Goudey plant simulation when the gas stream flowrates were mistakenly input in kg/hr rather than kg/s. This error resulted in the simulation not converging because of unreasonably high gas velocities at the inlet. Diagnostic messages were therefore added to warn the user when the inlet velocities, calculated from input flowrate values, exceed a reasonable value. A value greater than 200 m/s is currently considered unreasonable. Diagnostics were also added to aid the user in selecting the upper temperature limit for the physical properties table. The lower limit is fairly easy to select; it is commonly set equal to the lowest inlet stream temperature entering the reactor. The upper temperature limit is difficult to specify because some regions of the reactor may exchange significant heat

PARTICLES

LYPS : ☑ Uniform mass flux
LPARTS: ☑ Particles in Secondary
LSPU : ☑ No particles Axial Velocity Term
LSPH : ☑ No particles Energy Source Term
LPARTP: ☑ No particles in Primary
LSPM : ☑ No particles in Mass Source Term
LSPV : ☑ No particles Radial Velocity Term
LRBND : ☑ F

Number of particle trajectory starting locations	:	10
Number of particle sizes/types	:	5
Solids loading in primary	:	5.07955
Particle Density (kg/m^3)	:	1340.00000
Normalized upper bound for particle starting location:		0.950
Normalized lower bound for particle starting location:		0.020
Maximum number of particle phase iterations	:	15
Max. no. part. iter. for convergence	:	1

Index for gas property interpolation: ☑ Gas properties interpolated in both directions

Particles Initial Diameter units: ☑ m

1: 4.5e-05	2: 5.253-05	3: 6e-05	4: 6.75e-05
5: 7.5e-05	6: 0	7: 0	8: 0
	9: 0	10: 0	

Particle Properties: ☑ Different Particle Number: ☑ 1

Velocity	: 0.950000	units: ☑	m/s
Radial Position	: 0.000000	units: ☑	m
Temperature	: 1.000000	units: ☑	C
Mass Fraction	: 0.200000	units: ☑	m
Turbulent Pr/Sc	: 0.350000		

Figure III.A-21. Particle data window for the OPENLOOK Graphical user interface.

through radiation with other regions of the reactor. Therefore, the code was modified to print a message whenever the upper temperature limit specified by the user is inadequate and needs to be modified. The message also suggests what the new value should be.

Graphics - The various post-processors for plotting gas, particle, and pollutant properties were consolidated during the last year into a single program with various options. An option was added to the post-processor for producing text files in tabular format that can be read and plotted with a simple spreadsheet program. Options were also added for creating velocity vector plots and for comparing code predictions with experimental data. The data comparisons for gas composition can be made on either a wet or dry basis.

Foundational Code Specifications

Minimum specifications for a foundational, entrained-bed code that will satisfy the terms of the contract were identified. These specifications are as follows:

1. The percolation version of FG-DVC with rank-dependent kinetics will be included. Additional submodels from AFR will also be included based on availability.

2. The code will operate with a single solids progress variable. Coal offgas composition will be assumed constant. If possible, volatiles enthalpy will be allowed to vary as predicted by FG-DVC.

3. Code output will be provided in a format suitable for hardcopy printout. In addition, electronic data files suitable for use with independent computer graphics programs (e.g. spreadsheets and/or more advanced commercial software) for plotting will be provided, and experiences with such graphics programs will be documented. Any software (i.e. driver programs) developed under this program in connection with the use of such graphics programs will also be provided.

4. Sorbent injection will be allowable with the coal or through an additional, sidewall inlet.

In addition to identifying a set of minimum specifications for compliance with the contract, additional features that would further enhance code performance were identified. These additional features will be considered once the development of a code with the minimum specifications is insured, based on availability of resources and technology. The additional features include

additional submodels, an additional solids progress variable for tracking coal offgas, and aft injection of coal. The latter has been incorporated under Subtask 3c.

Plans

During the next quarter, the final version of the FG-DVC submodel will be integrated. Other submodels from Task 2 (e.g. swelling and char reactivity) will be incorporated if available. Evaluation cases will be run with the FG-DVC submodel and compared with experimental data. Additional cases of the ABB CE drop-tube furnace will be run. A coal combustion case in the CPR will be run. The TWR cases will be completed. Effort will be made to resolve the problems with the Imperial College simulations. Further consideration will be given to incorporating energy feedback from volatile flames. Work will continue on code graphics.

III.B. SUBTASK 3.B. - COMPREHENSIVE FIXED-BED MODELING, REVIEW, DEVELOPMENT, EVALUATION, AND IMPLEMENTATION

Senior Investigators - Predrag T. Radulovic and L. Douglas Smoot
Brigham Young University
Provo, Utah 84602
(801) 378-3097 and (801) 378-4326

Research Assistant - M. Usman Ghani

Objectives

The objectives of this subtask are: 1) to develop an advanced, fixed-bed model incorporating the advanced submodels being developed under Task 2, particularly the large-particle submodel (Subtask 2.e.), and 2) to evaluate the advanced model.

Accomplishments

During the past year, work continued on developing and evaluating the fixed-bed model. The first version of the one-dimensional, fixed-bed model, MBED-1, was finalized and evaluated by simulating several test cases and comparing predictions with experimental data. The user's manual for the MBED-1 code was completed and reviewed. The MBED-1 code and user's manual were submitted to METC. The minimum specifications for the final fixed-bed code, FBED-1, and the cases for the application of the code were defined and accepted by both AFR and METC. A major improvement in the FBED-1 code is the inclusion of the FG-DVC submodel developed at AFR. The stand-alone FG-DVC submodel was received from AFR and studied in detail for better understanding and proper integration in the final version of the comprehensive, fixed-bed code. Preliminary integration of the FG-DVC submodel was performed jointly by BYU and AFR, but was only partially successful. This effort necessitated restructuring of the final version of the code. The present version of the fixed-bed code, FBED-1, which includes the properly integrated FG-DVC percolation submodel, was tested by simulating a Wellman-Galusha gasifier fired with Jetson bituminous coal. The results compared well with the previous versions of tne

fixed-bed code. Two papers were submitted for publication (Hobbs et al., 1991a, 1991b).

Preliminary Code Version (MBED-1)

Evaluation – The first version of the fixed-bed code, MBED-1, was further evaluated by simulating several test cases for a Wellman-Galusha gasifier fired with Elkhorn bituminous, Jetson bituminous, Leucite Hills bituminous, and Utah Blind Canyon bituminous coals. Figure III.B-1 compares the predicted and measured temperature profiles and shows the effect of operating conditions for these four coals. Additional evaluation was performed, by studying the mathematical models and the computational methods which form the theoretical basis of the code and through a line-by-line check of the code. Portions of the code which can be rewritten as separate modules were identified. The robustness of the code was tested by applying the code to a limiting case of devolatilization under an inert environment. The results did not produce a converged solution, and the portions of the code were identified which need to be improved to yield converged results under all conditions. A brief discussion of the Wellman-Galusha simulation results follows.

Elkhorn Bituminous Coal Case - A shift in the measured temperature profile due to changing reactant feed rates during gasification of Elkhorn bituminous coal is shown in Figure III.B-1A. The predicted trends were in agreement with the direction of the measured temperature shifts in each case. From the sensitivity analysis, an increase in coal flow rate caused the location of the maximum temperature to move closer to the bottom of the reactor. In general, an increase in either the steam flow rate or air flow rate caused the location of the maximum temperature to move closer to the top of the reactor. In this case, the coal and air flow rates were increased, the steam flow rate was decreased, and the location of the maximum temperature moved toward the reactor bottom. Although increased air flow rate would cause the location of the maximum temperature to move toward the reactor top, changes in coal and steam flow rates were apparently more significant for the Elkhorn case.

Jetson Bituminous Coal Case - The effect of varying operational parameters on the location of the maximum temperature is shown in Figure III.B-1B for gasification of Jetson bituminous coal. The direction of the temperature

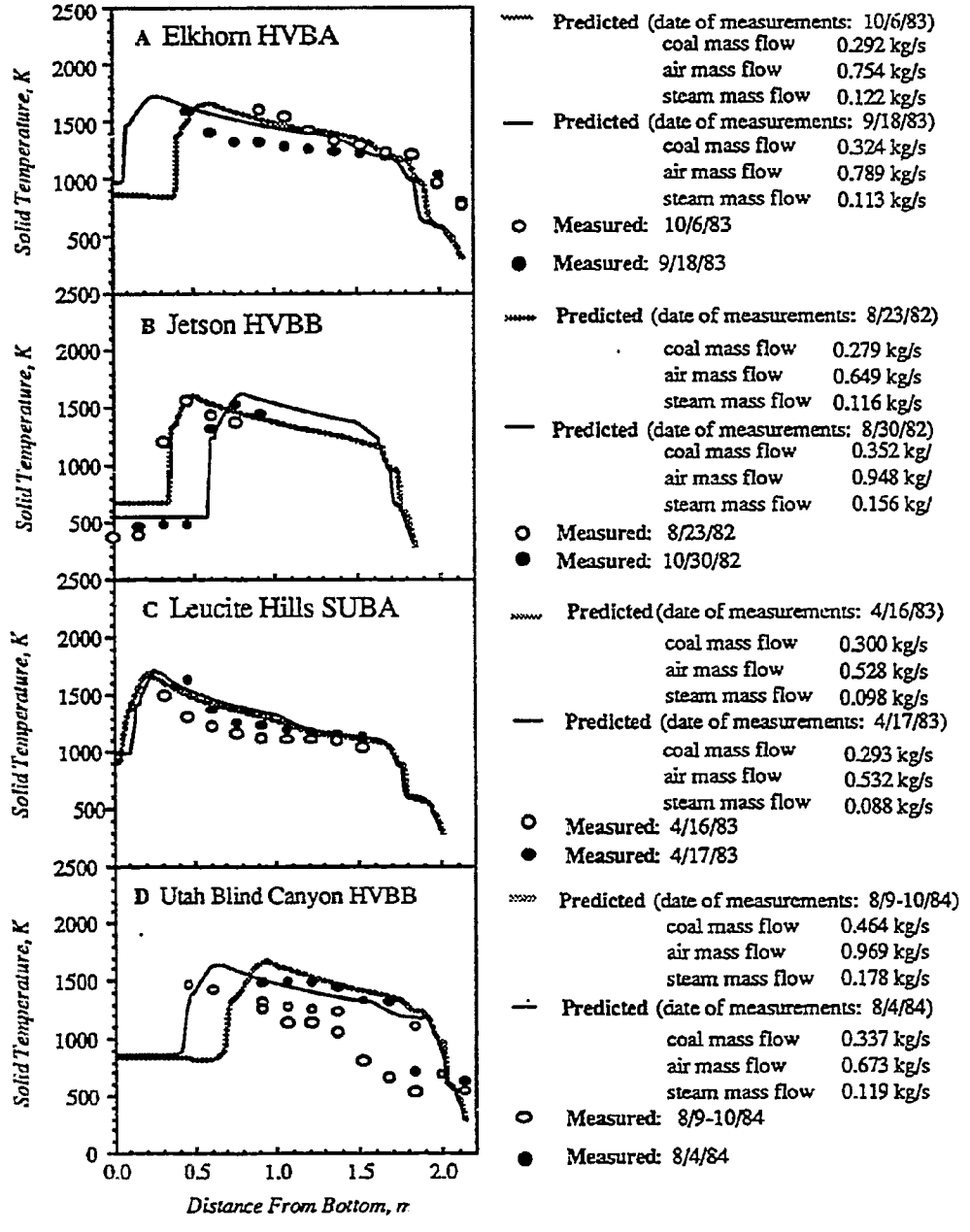

Figure III.B-1. Comparison of measured temperature and predicted solid temperature for gasification of several coals in an air-fired, low pressure Wellman-Galusha gasifier. Experimental data can be found in Thimsen et al. (1984).

shift was predicted adequately by the one-dimensional model. An increase in the coal, air and steam mass flow rates caused the location of the maximum temperature to move toward the top of the reactor. For the Jetson case, the increases in steam and air mass flow rates were apparently more significant than the increase in the coal mass flow rate.

Leucite Hills Subbituminous Coal Case - Although gasification of low-rank coals seems to be more difficult to simulate, predictions from the one-dimensional model were in agreement with the experimental data for the Leucite Hills subbituminous coal, as shown in Figure III.B-1C. The increase in coal flow rate and decrease in steam flow rate caused the location of the maximum temperature to shift toward the bottom of the reactor for the Leucite Hills case.

Utah Blind Canyon Bituminous Coal Case - The Utah Blind Canyon case depicted in Figure III.B-1D also shows the effect of increased coal and gas throughputs. Trends in measured and predicted profiles do not agree for this case. The uncertainty in the experimental measurements may explain the discrepancy. The temperature measurements were taken for two time periods. For the first time period, the measurements were repeated on two separate days, but only one set of operational data was reported for this time period (Thimsen et al., 1984).

Documentation and Implementation – A user's manual for MBED-1 (which includes only the FG submodel) was prepared. The manual consists of two parts. The first part includes the model formulation and the solution procedure, whereas the second part includes user's and implementation guides as well as sample problems. The first version of the one-dimensional code, MBED-1, includes only the FG submodel. The code was ported to a Silicon Graphics workstation, and a sample case was successfully executed. The sample case was for the Wellman-Galusha gasifier fired with the Jetson bituminous coal. The code, user's manual, and installation instructions were sent to METC.

Final Code Version (FBED-1)

Minimum specifications for the final product version of the fixed-bed code (FBED-1) were approved by both AFR and METC. They include:

1. One-dimensional, heterogeneous, counter-flow, steady-state.
2. Gas flow calculated by Ergun equation; solid flow with variable velocity and porosity.
3. Bed settling with variable porosity.
4. Solid-to-gas heat transfer with effective heat transfer coefficient.
5. Devolatilization calculated by FG-DVC percolation submodel for large particles.
6. Combustion/gasification with shell-progressive shrinking core (SP) or ash segregation (AS) submodel.
7. Gas chemistry by partial equilibrium.
8. Code output will be provided in a format suitable for hardcopy printout. In addition, electronic data files suitable for use with independent computer graphics programs for plotting will be provided.

The code plan and schedule with milestones for completing the contract were also proposed and accepted at the Contract Review Meeting in March.

FG-DVC Submodel – Coal devolatilization in MBED-1 is based on the Functional Group (FG) model along with computation of the tar yield based either on the correlation of Ko et al. (1988) or as specified by the user. The simulation results show a significant effect of tar yield and demonstrate the need for a more rigorous devolatilization model. A major improvement in FBED-1 is that devolatilization modeling is based on the full FG-DVC submodel. FG-DVC was developed on a Sun workstation under an older version of the operating system (Sun OS 3.4). The code was ported to a Sun workstation at BYU under Sun OS 4.1, and a sample case was executed with partial success. The stand-alone FG-DVC code, modified to exclude graphics routines, was executed successfully. The differences in the graphics routines between the two operating systems, Sun OS 3.4 and Sun OS 4.1, are. The code with the graphics routines was, therefore, not executed. The most recent version of FG-DVC is formulated as a differential equation system. The original version was formulated as an algebraic equation system.

Code Development – The preliminary integration of the FG-DVC submodel into the comprehensive fixed-bed code was performed jointly by BYU and AFR. The number of functional groups in the fixed-bed code was increased from 19 to 27. Furthermore, these functional groups are tracked in the char, tar and gas

phases. The new version includes rank-dependent devolatilization kinetics. The preliminary integration of FG-DVC was performed by adding the new devolatilization equations and then tracking tar and the original nineteen functional groups of the MBED-1 model. A sample case for the Wellman-Gallusha gasifier fired with Jetson bituminous coal was simulated, but with only partial success; the integration broke down in the oxidation zone, as shown in Figure III.B-2. It is interesting to note that the pressure, major and minor species concentrations, particle diameter and burnout do not show any discontinuities. It is only the temperature profiles and, in particular, the carbon consumption rates, which clearly demonstrate the breakdown.

In order to isolate and correct the problem, two possibilities were explored. The first one was to determine if the FG-DVC submodel was the source of the error. This was achieved by allowing devolatilization to occur in the drying, devolatilization and gasification zone but not in the oxidation zone. This did not correct the problem, and therefore, this possibility was ruled out. The second one was to determine if the inherent, non-linear nature of the system of ordinary differential equations was the cause of the problem. Simulations were made with the standard LSODE integration package instead of the sparse version, LSODES, as well as with a simpler 5th-6th order Runge-Kutta-Felhberg algorithm with step-size control. Both of these approaches required some adjustment of tolerances, but were successful, and integration in the oxidation zone proceeded without any discontinuities. The CPU time requirements with the standard LSODE integration were significantly less than that needed for the Runge-Kutta-Felhberg algorithm. The results of a simulation for the Wellman-Galusha gasifier, using the standard LSODE package, are shown in Figure III.B-3.

The preliminary version of the FBED-1 code included twenty redundant equations for the nineteen functional groups and the tar-forming fraction, and therefore, a complete restructuring of the code was required to eliminate this redundancy. A significant aspect of the code restructuring was the rearrangement of the system of governing equations. This rearrangement was achieved by separating the governing equations into two groups. The first group is comprised of the equations which must be solved irrespective of the choice of devolatilization submodel. The second group is comprised of the equations which depend upon the choice of devolatilization submodel. In the modified setup, tar in the gas phase is treated as a pseudo-phase, and the equations within these

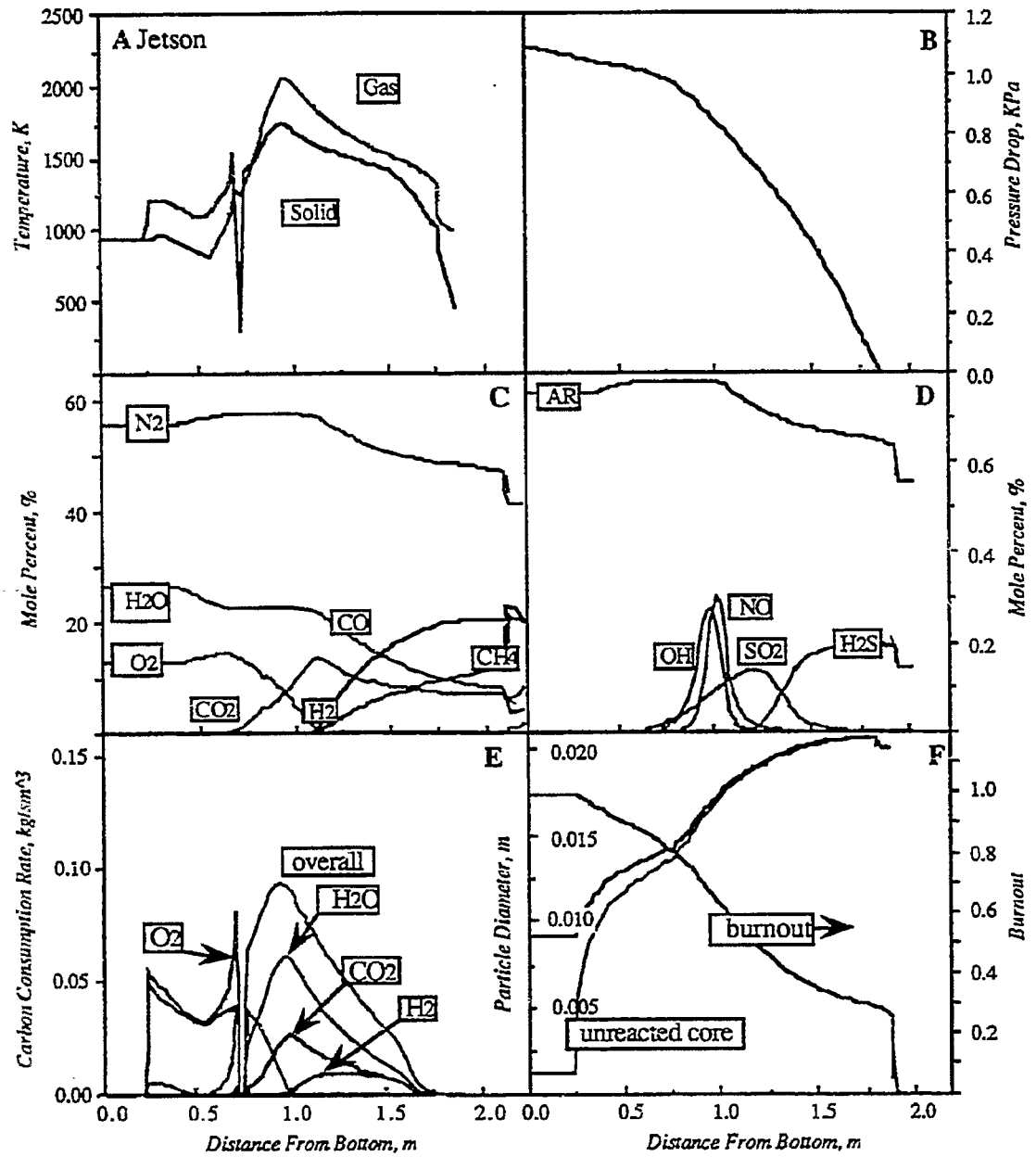

Figure III.B-2. First FBED-1 predicted axial A) temperature, B) pressure drop, C) major species concentration, D) minor species concentration, E) oxidation/gasification carbon consumption rate, F) burnout, overall and unreacted particle diameter in an atmospheric, air-blown Wellman-Galusha gasifier fired with Jetson bituminous coal. Input parameters given in Thimsen et al. (1984, volume 2, page K5).

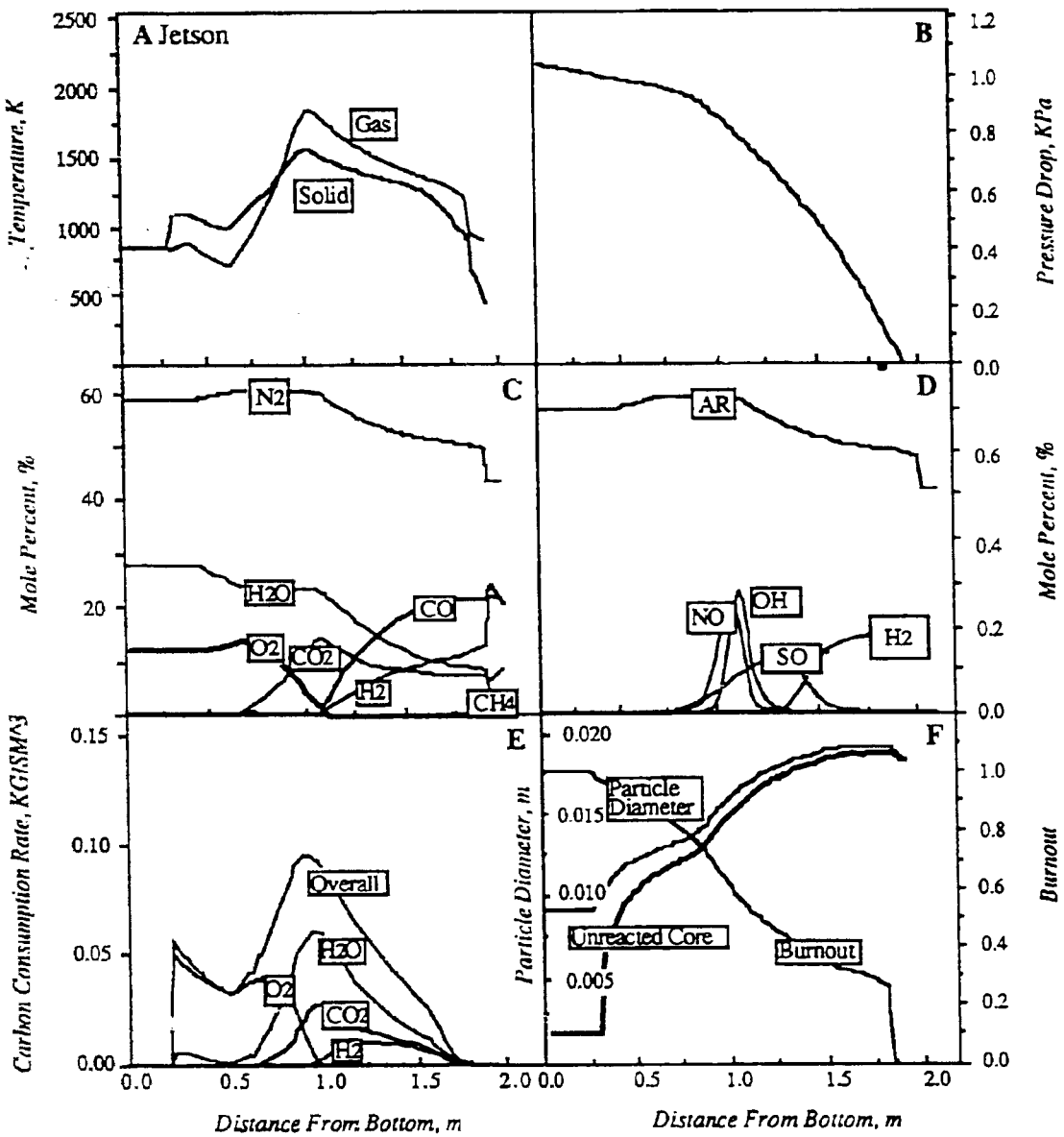

Figure III.B-3 Preliminary FBED-1 predicted axial A) temperature, B) pressure drop, C) major species concentrations, D) minor species concentrations, E) oxidation/gasification carbon consumption rate, F) burnout, overall and unreacted particle diameter in an air-blown, atmospheric Wellman-Galusha gasifier fired with Jetson bituminous coal.

two groups were further arranged in a logical order dealing with separate gas, tar and solid phases. The new setup permits inclusion of additional variables and corresponding governing equations with minimal changes in the code and is, therefore, considered a major improvement in the code structure.

The MBED-1 code was used to test the new structure of the code. Simulations were made for the Wellman-Galusha gasifier fired with Jetson bituminous coal with both versions (i.e., the original and the restructured versions), and the results were compared. The two versions did not produce identical results. The values of all the output variables, however, were always very close and usually differed only after the 3rd or 4th significant digit. A careful scrutiny of the modified version of the code did not reveal any errors in coding. Experimentation with step size and tolerances did not yield any improvements in the results and, instead, showed some effects of these integration parameters. However, no discrepancies in the results of the zero-dimensional portions of the codes, which do not involve any integration, were observed. In order to identify the problematic module, the two versions were executed with the Runge-Kutta-Felhberg integration routine, and they produced identical results. It was therefore concluded that the standard LSODE integration routines were the source of the problem and should be carefully studied.

The new version of the MBED-1 code formed the foundation for the present version of the FBED-1 code, which is fully restructured to properly integrate the FG-DVC percolation submodel. The FG-DVC submodel, provided by AFR was modified to accommodate the new structure of FBED-1. Options were added in the FBED-1 code to perform the numerical integration of the resulting system of equations using the LSODE or the Runge-Kutta-Felhberg algorithm with step-size control. Portions of the code were also rewritten to enhance clarity and modularity. The code was executed on a Sun Sparc station 1 computer. A sample run for the Wellman-Galusha gasifier fired with Jetson bituminous coal was made, and the results are shown in Figure III.B-4.

The results from the preliminary and the current versions of FBED-1 are similar but there are also differences as one can see in Figures III.B-3 and III.B-4. Some of these differences can be attributed to the coding errors found in the preliminary version. Others remain to be explained. There are also

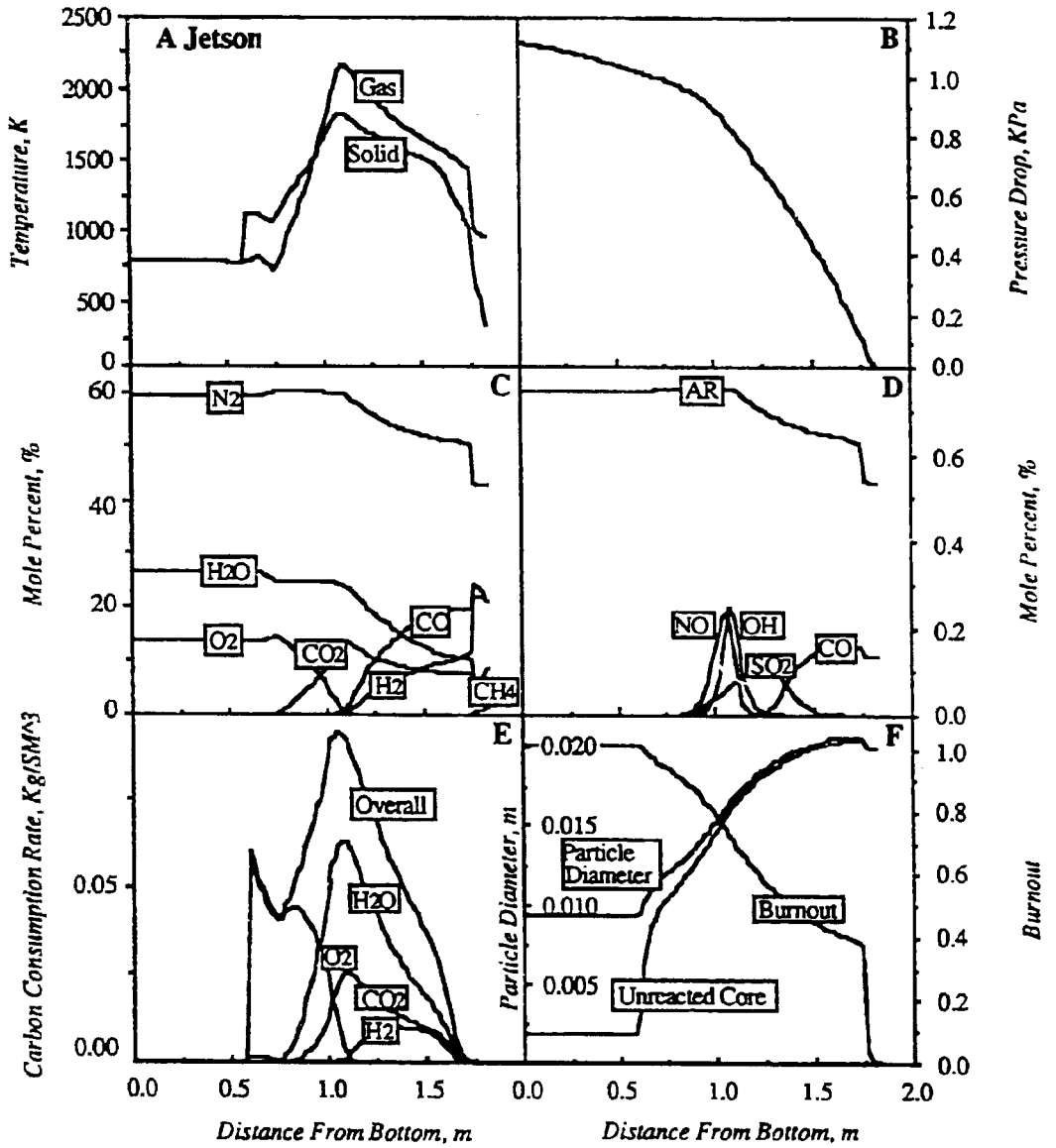

Figure III.B-4 Current FBED-1 predicted axial A) temperature, B) pressure drop, C) major species concentrations, D) minor species concentrations, E) oxidation/gasification carbon consumption rate, F) burnout, overall and unreacted particle diameter in an air-blown, atmospheric Wellman-Galusha gasifier fired with Jetson bituminous coal.

questions with both versions of the code. The comparison of predictions with Wellman-Galusha data for the Jetson coal case are currently better with the completed MBED-1 code than with the preliminary FBED-1 code, as shown by Figures III.B-3 and III.B-4. In preliminary FBED-1 predictions, questions include high ash and maximum temperatures, dips in temperatures and a jump in oxygen between the ash and the oxidation zone, a jump in nitrogen in the oxidation zone, etc. These questions are probably numerical in origin and remain to be resolved.

The current version of FBED-1 was also ported to a VAX computer running under the VMS operating system. The code was compiled successfully, but twenty-five warning messages were given. These messages were related to the character variables in the module CREEO, which were initialized in data statements with Hollerith variables. In addition, two minor modifications had to be made in the code: the machine-dependent routine ETIME was replaced with the equivalent routine SECNDS on the VAX, and calls to the routine FLUSH were commented out. The code was executed successfully after making these minor modifications. The results, although very close, were not identical to the results on the Sun machine. The differences may be attributed to the hardware differences of the two machines.

Plans

During the next quarter, work will continue on developing the final version of the comprehensive, fixed-bed model, FBED-1. Additional portions of the code will be rewritten to further improve code structure, modularity and user-friendliness. All submodels will be thoroughly studied to justify their inclusion in the final code. Options will be provided in the code to choose between the simpler FG model or the more rigorous FG-DVC model. The iteration method will be further modified to improve convergence and robustness. The fixed-bed code will then be validated, and a sensitivity analysis will be performed. Work on spreadsheet graphics and other graphic outputs/interfaces will be initiated. Preparation of the FBED-1 user's manual will be initiated.

III.C. SUBTASK 3.C. - GENERALIZED FUELS FEEDSTOCK SUBMODEL

Senior Investigators - B. Scott Brewster and L. Douglas Smoot
Brigham Young University
Provo, UT 84602
(801) 378-6240 and 4326

Objective

The objective of this subtask is to generalize PCGC-2 to include sorbent injection, as outlined in the Phase II Research Plan.

Accomplishments

PCGC-2 was modified to allow both coal and sorbent particle injection in secondary and additional (sidewall) inlets. The method of calculating the source term for the gas phase based on sulfur capture by sorbent was verified.

Plans

Test modifications with coal and/or sorbent particles in additional (sidewall) inlets.